Multi-level orchestration of γδ T cell development and central nervous system inflammation by retinoic acid

Marcelo Gregorio Filho Fares da Silva[1*], Rasmus Agerholm[1*], Nital Sumaria[3], John Rizk[2], Julia Fiske[1], Elisa Catafál-Tardos[1], Maria Virginia Baglioni[1], Davide Secci[1], Paula Peñalver Sebastián[1], Daniel Pennington[3] and Vasileios Bekiaris[1**]

[1]Department of Health Technology, Technical University of Denmark, Kemitorvet, Bldg 202, 2800 Kgs Lyngby, Denmark.

[2]Department of Immunology and Microbiology, LEO Foundation Skin Immunology Research Center, University of Copenhagen, Copenhagen, Denmark

[3]Blizard Institute, Barts and The London School of Medicine, Queen Mary University of London, 4 Newark Street, London E1 2AT, UK.

*These authors contributed equally

**Address correspondence to Vasileios Bekiaris vasbek@dtu.dk

Abstract

The vitamin A metabolite retinoic acid (RA) is critical for the maturation and function of the immune system, however, our knowledge regarding its role in gamma delta (γδ) T cells is limited. By specifically inactivating the RA receptor alpha (RARα) in type 3 lymphocytes and using a combination of fetal thymic organ cultures and single-cell RNA-sequencing we found that RA strengthened TCR signaling to limit the embryonic development of interleukin(IL)-17-producing γδ T cells (γδT17), while at the same time it promoted their survival after birth. In adult mice, RA imposed a multi-level transcriptional program allowing γδT17 cells to become activated, survive and sense interferon. Consequently, cells with inactive RARα responded poorly to immunization and produced low level of cytokines leading to near disease resistance in the experimental autoimmune encephalomyelitis model. Finally, RA was required for optimal expression of the α4β1 integrin and γδT17 cell infiltration to the brain. Collectively, these studies suggest that by acting at various stages during the lifetime of γδ T cells, RA supports their normal development, their survival and their ability to respond to inflammatory stimuli.

Introduction

Gamma delta (γδ) T cells are innate-like lymphocytes, evolutionary conserved from lampreys to humans (*1, 2*). They are critical for effector immunity against many pathogens and cancers, but also have key tissue homeostatic functions, while in chronic inflammation they can become highly pathogenic (*3*). Similar to other lymphocytes, γδ T cells can be defined in subsets based on the type of immune responses they participate in and elicit, such as type 1 interferon(IFN)-γ-producing (γδT1) or type 3 interleukin(IL)-17-producing (γδT17) (*4*). Mouse γδT17 cells start to develop around embryonic day 16 (e16) through a combination of signals from the T cell receptor (TCR) and the transcription factors cMAF and RORγt. Thus, γδ T cell committed progenitors that have avoided Skint-1 selection (*5*), require weak TCR signals (*6, 7*) to differentiate into cMAF-expressing cells, a step important for their commitment into fully functional RORγt$^+$ type 3 effector cells (*8*). Right before and right after birth γδT17 cells are exported from the thymus to secondary lymphoid organs (SLOs) and most epithelial and barrier surfaces (*9*). During the first week of life STAT5 is required to sustain γδT17 survival and proliferation within tissues (*10*), while continuous suppression of the non-canonical NF-κB pathway by the E3 ligases cIAP1 and cIAP2 maintains expression of cMAF and RORγt and allows further expansion after weaning (*11*). Thus, sequential embryonic and neonatal checkpoints ensure the lineage stability of γδT17 cells.

In addition to their seemingly pre-programmed phenotype and function, γδT17 cells acquire tissue-specific properties, such as type 1 effector functions in the gut (*10, 12*), or thermoregulation in adipose tissue (*13*). In muscle, γδT17 cells promote tissue regeneration following injury (*14*) and in the brain they appear to be important for maintaining short-term memory (*15*) and to regulate anxiety-like behavior (*16*). Collectively, these data suggest that γδT17 cells can sense and adjust to their microenvironment, likely by responding to local metabolites. In this regard, we reasoned that dietary associated metabolic products, such as vitamin derivatives, could be critical for the development and functional maturation thereafter of γδT17 cells.

Vitamin A is a natural retinoid that can only be obtained through the diet and is necessary for normal human development (*17*). Pre-formed dietary retinoids, mainly retinol and retinyl esters, or proretinoids like β-carotene are absorbed in the gut and after a series of hydrolysis and esterification reactions are packed into chylomicrons, and through the lymphatic system are

primarily transported to the liver where they are stored (*18*). Retinol packed in the liver is transported to peripheral tissues via retinol binding proteins and upon cellular uptake it can get oxidized by aldehyde dehydrogenases into its main active metabolite retinoic acid (RA) (*18, 19*). Cellular RA binding proteins relocate RA from the cytosol to the nucleus where it will interact with RA receptor (RAR)-retinoid X receptor (RXR) dimers (*18, 20*). The RAR-RXR complex may be composed of any of three RARs, RARα, RARβ, RARγ, which are mostly ubiquitously expressed, but can show tissue specificity (*21, 22*). The RAR-RXR dimer functions as a transcriptional regulator, which upon binding to RA releases its associated co-repressors, recruits co-activators and initiates gene transcription through recognition of RA response elements (RARE) (*21-23*). RAREs are dispersed throughout the genome on promoters, enhancers and intragenic regions and regulate thousands of genes that result in pleiotropic biological effects ranging from neuronal development to bone morphology (*20, 24, 25*). Vitamin A and RA are also very important for the development and function of our immune system (*17*). Thus, RA promotes the formation of SLOs (*26, 27*) during embryogenesis, it induces expression of the gut homing molecules CCR9 and α4β7 on T cells and innate lymphoid cells (*28-30*) and is critical for the differentiation of T-helper (T_H) cells and the balance between T_H cell subsets (*31-35*). Furthermore, RA regulates T_H1 to T_H17 plasticity (*36*) and is critical for the development of small intestinal intra-epithelial lymphocytes (*37, 38*), while more recent data showed the importance of RA in establishing tissue resident memory cells (*39, 40*). Although treatment of cells or mice with synthetic RA can regulate some functions of γδ T cells (*41, 42*), the intrinsic requirements for RA in this cell population has not been elucidated.

Herein we provide evidence that RA is a key molecular determinant throughout the life of γδT17 cells. We show that during embryonic life, RA strengthens the TCR signal to limit γδT17 generation; during neonatal life RA is important for survival, while during adult steady-state conditions it maintains γδT17 numbers in SLOs. In the context of central nervous system inflammation, modelled by autoimmune experimental encephalomyelitis (EAE), RA is necessary to sustain γδT17 cells and their ability to produce cytokines, as well as to accumulate in the brain. Through combined defects in the T_H17 compartment, mice with impaired RAR activity in type 3 lymphocytes show near complete resistance to EAE symptoms.

Results

RA limits the development of γδT17 cells

In order to test the intrinsic importance of RA in γδT17 cells we crossed RORγt-Cre recombinase^{+} mice (RORγt^{CRE}) (*43*) with mice whereby constitutive expression of a RARα dominant negative (dn) transgene within the *ROSA26* locus was prevented by a floxed stop codon (RARdn$^{F/F}$) (*44*). Excision of the stop codon allowed constitutive RARdn transgene expression, preventing endogenous RARα from becoming activated (*44*) (**Fig. 1A**). Using RORγt^{CRE}-RARdn$^{F/F}$ mice (referred to thereafter as Cre^{+}) and their Cre^{-} littermate controls we first assessed whether RA is implicated in thymic development. Embryonic thymic γδT17 cells were identified as CD24^{-}CD27^{-}CD45RB^{-}CD44^{+} (*6*), and in the neonates as CD27^{-}CD44^{+} (*4*) and were split into Vγ4^{+} and Vγ4^{-} (Vγ nomenclature according to Heilig & Tonegawa (*45*)) (**Fig. S1A**). At embryonic day e18 total γδ T cells were not affected by inactive RARα (**Fig. S1B**), however, we found that numbers of γδT17 cells, of which approximately 90% were Vγ1/4^{-} (**Fig. S1C**), were elevated, albeit not significantly (**Fig. S1D**). At that point, very few Vγ4^{+} cells could be detected and their numbers were unchanged (**Fig. S1D**). One day after birth, throughout neonatal life and until weaning at 3 weeks, the numbers of Vγ4^{-} γδT17 cells were increased in Cre^{+} thymi (**Fig. S1E**). Of note, while the numbers of Cre^{-} Vγ4^{-} γδT17 cells plummeted shortly after birth, Cre^{+} cells persisted in the thymus for 2-3 weeks (**Fig. S1E**). There were no observable changes in Cre^{+} Vγ4^{+} cells up until day 21 after birth, at which point their numbers indicated a small decline (**Fig. S1E**).

The increased numbers of Vγ4^{-} γδT17 cells both in embryonic and neonatal thymus suggested that RA may negatively regulate the development of these cells. In order to start gaining mechanistic insights that explained this phenotype, we set up fetal thymic organ cultures (FTOCs) as previously described (*6*), in the presence or absence of a synthetic RARα inhibitor (**Fig. S1F**). We found that RARα inhibition promoted the generation of higher numbers of γδT17 cells (**Fig. S1G**), which under these conditions are dominated by the Vγ4^{-} subset (*6*). However, exogenous high concentration of RA in the culture with all-trans RA (ATRA) did not reduce γδT17 cell numbers (**Fig. S1H**). Collectively, these data show that impaired sensing of RA favors thymic output of γδT17 cells and suggest that sustained RARα activity may limit their embryonic development.

117 **RA sustains multiple transcriptional programs during γδT17 cell development**

118 The above data prompted us to further investigate how RA may influence the biology of γδT17
119 cells during embryonic and early life development. To this end, we isolated γδT17 cells from e18
120 and newborn Cre$^-$ or Cre$^+$ thymi (see gating strategy in **Fig. S1A**) and performed single-cell RNA-
121 sequencing experiments (scRNA-seq). We used Uniform Manifold Approximation and Projection
122 (UMAP) analysis to visualize γδT17 cells by integrating both time points and genotypes.
123 Unsupervised clustering showed 13 clusters, 5 unique to e18 (c3, c6, c7, c8, c12), 7 unique to
124 newborn (c0, c1, c2, c4, c5, c10, c11) and one cluster (c9) that was common (**Fig. 1B and Table**
125 **S1**). Expression of signature γδT17 genes such as *Rorc*, *Zbtb16* and *Maf* was found in all clusters,
126 while the majority of cells expressed *Trgv6* in line with Vγ6$^+$ cells being more abundant in the
127 thymus at these stages of life (**Fig. 1C**). *Trgv4* expressing cells were found mostly in cluster c9,
128 which in newborn mice was almost entirely derived from Cre$^-$ cells (**Fig. 1D-E**). Although this
129 suggested that RA supported the early development of Vγ4$^+$ cells, their numbers were not affected
130 in either e18 or newborn Cre$^+$ thymus (**Fig. S1D-E**).

131 Next, we investigated differentially expressed genes (DEGs) for both e18 and newborn
132 thymus between Cre$^-$ and Cre$^+$ cells. At e18 there were 43 genes downregulated and 3
133 upregulated in Cre$^+$ cells, while in the newborn there were 90 genes downregulated and 20
134 upregulated in Cre$^+$ cells (**Fig. 1F-G and Table S2**). Some of the downregulated genes at e18 but
135 not newborns included the AP-1 transcription factors *Jun* and *Fos* and the signaling molecules
136 *Dusp1*, *Map3k5* and *Tnfaip3*, as well as *Il17a* and *Cd69* (**Fig. 1F-G**). Both embryonic and newborn
137 thymic Cre$^+$ cells had reduced levels of *Tnfsf11* (RANKL) and *Vsir* (VISTA) while newborn Cre$^+$
138 cells had reduced *Adgre5* (CD97), *Cd226*, *Vdr*, and *Stat4* (**Fig. 1F-G**), suggesting a more
139 generalized defect in T cell function. The gene coding the transcription factor KLF2 was also
140 downregulated in both embryonic and newborn Cre$^+$ cells, while its target *S1pr1*, which promotes
141 thymic egress (*46*), was additionally decreased in newborn Cre$^+$ thymocytes (**Fig. 1F-G**). Notably,
142 Cre$^+$ cells had downregulated many genes of the GIMAP family (e.g. *Gimap1*, *Gimap4*, *Gimap5*),
143 especially in the newborn (**Fig. 1F-G**). GIMAPs are GTPases implicated in the development and
144 differentiation of T cells and have potent pro-survival and anti-apoptotic roles (*47*). In line with this,
145 the gene coding the anti-apoptotic molecule Bcl-2 was also downregulated in the absence of active

146 RARα in the embryo and newborn (**Fig. 1F-G**). Collectively, in the embryonic and newborn thymus
147 RA regulates a transcriptional program in γδT17 cells related to multiple signaling pathways, tissue
148 homing and retention as well as cell survival.
149
150 **RA strengthens the TCR signal during embryonic γδT17 cell development**
151 Next, we wanted to understand how can the above transcriptional changes explain the increased
152 thymic output of γδT17 cells in mice with inactive RARα. We noted that the genes *Jun*, *Fos*, *Dusp1*
153 and *Map3k5*, which have all been implicated in TCR signaling, were specifically downregulated in
154 Cre^+ e18 cells (**Fig. 1F-G**). We additionally found that cluster c12 separated from the rest based on
155 1351 DEGs, a large proportion of which appeared to be associated with cellular signaling, such as
156 *Cblb*, *Malt1*, *Fyn*, and *Traf3* (**Table S1**). We then used over-representation analysis (ORA) to test
157 whether the genes in cluster c12 enriched specific signaling cascades of immunological
158 importance, and found that the TCR signaling pathway was the most highly and significantly
159 enriched (**Fig. 2A**). Furthermore, cluster c12 was unique to e18 thymocytes and it was almost
160 absent in Cre^+ cells (**Fig. 2B and Fig. 1B**). Thus, these data indicate that RA is important in the
161 embryonic thymus to induce genes that are corelated with TCR induced pathways.
162 The above led us to hypothesize that RA through RARα may regulate TCR signaling. To test
163 this hypothesis, we set up FTOCs in the presence of a RARα inhibitor and the agonistic anti(α)-
164 TCRγδ GL3 Ab, which triggers the TCR and suppresses γδT17 development (*6, 48*). The surface
165 nucleotidase CD73 can be used as a surrogate marker to indicate TCR activity in early γδ T cell
166 committed progenitors (*49*). α-TCRγδ stimulation induced expression of CD73 in both immature
167 $CD24^+$ γδ T and committed γδT17 cells, which was antagonized by RARα inhibition (**Fig. 2C-D**),
168 and under these conditions, γδT17 output was partially rescued (**Fig. 2E**). In contrast, addition of
169 ATRA increased surface expression of CD73 in both $CD24^+$ γδ T (**Fig. 2F**) and γδT17 cells (**Fig.
170 2G**). Collectively, these data show that impaired RA sensing attenuates TCR signaling in
171 embryonic life and help explain the increased numbers of γδT17 in Cre^+ thymi. Our findings
172 suggest that under normal conditions RA strengthens TCR signaling in the embryonic thymus,
173 limiting thus the development of γδT17 cells.
174

175 **RA promotes survival and represses apoptosis of neonatal γδT17 cells**

176 Attenuated TCR signaling helps explain the increased numbers of γδT17 cells in the embryonic
177 and neonatal thymus. However, higher thymic output did not translate into higher numbers in the
178 periphery. In contrast, Vγ4^{-} γδT17 numbers were not increased in the neonatal lymph nodes
179 (LNs), while the numbers of Vγ4^{+} γδT17 cells were significantly reduced at 2 and 3 weeks after
180 birth (**Fig. S2A**). Furthermore, adult Cre^{+} LNs contained normal numbers of Vγ4^{-} and reduced
181 numbers of Vγ4^{+} cells (**Fig. S2B**), and in the adult spleen the numbers of both subsets were
182 significantly reduced (**Fig. S2C**). We therefore hypothesized that there must be a compensatory
183 mechanism by which the numbers of overtly generated γδT17 cells return to baseline or below. As
184 we saw GIMAPs and *Bcl2* being downregulated in newborn Cre^{+} cells, we speculated that RA
185 additionally supports survival and that when its sensing is inefficient, cells die at a higher rate
186 under homeostatic conditions.

187 We initially examined in detail the DEGs (see **Table S2 and Fig. 1F-G**) between Cre^{-} and
188 Cre^{+} cells at e18 and newborn thymus in order to pinpoint genes that have been reported before in
189 the literature to have anti- or pro-apoptotic properties (**Table S3**). We identified 24 genes with anti-
190 and 7 genes with pro-apoptotic properties and 3 with both (**Fig. 3A**). The majority of anti-apoptotic
191 genes were differentially and highly expressed in Cre^{-} cells of newborn origin, although this was
192 also true for the pro-apoptotic genes (**Fig. 3A**), indicating that RA is impacting the survival of
193 γδT17 cells. As Bcl-2 is a key pro-survival and anti-apoptotic molecule, we then determined its
194 protein levels in the thymus and LNs of newborn and neonatal mice. We found that Bcl-2 levels
195 were significantly reduced in Vγ4^{-} and Vγ4^{+} γδT17 cells that could not sense RA (**Fig. 3B**). To
196 investigate whether reduced levels of Bcl-2 were related to weaker TCR signals, we cultured
197 newborn thymocytes with α-CD3 in an attempt to restore the TCR signal strength. We found that α-
198 CD3 treatment induced Bcl-2 levels in Cre^{+} cells (**Fig. 3C**), suggesting that weak TCR signaling
199 may contribute to impaired survival. To formally test whether RARα inactivity resulted in increased
200 cell death, we analyzed the expression of the execution caspases 3 and 7. In order to induce
201 measurable levels of apoptosis we stressed newborn thymocytes by culturing them in vitro for 40
202 hours in the absence of any survival factors. Under these conditions, we found a higher proportion
203 of caspase 3/7 positive Cre^{+} γδT17 cells (**Fig. 3D**). Collectively, our data show that RARα sustains

204 the survival of newly generated γδT17 cells and indicate that this is linked to its ability to regulate
205 the strength of the TCR.
206
207 **RA induces activation, survival and interferon gene signatures in inflammation**
208 Next, we wanted to investigate whether RA is also required in γδT17 cells during inflammatory
209 responses. As γδT17 cells, in particular Vγ4$^+$, are important for the development and progression
210 of MOG-induced EAE (*50*), we isolated γδT17 cells from the spleens of Cre$^-$ and Cre$^+$ mice that
211 were either unimmunized (day 0, d0) or had been immunized 11 days prior (d11), performed
212 scRNA-seq, and analyzed Vγ4$^+$ and Vγ6$^+$ cells separately. By integrating both time points and
213 genotypes, we identified 7 Vγ4$^+$ clusters (**Fig. 4A**), all of which expressed type 3 genes (e.g. *Rorc*,
214 *Maf*, *Il23r*), and none expressed *Cd27*, a marker of type 1 cells (**Fig. 4B and Table S4**). All
215 clusters expressed *Trdv2-2*, except cluster c3 which was *Trdv5*$^+$ and had the lowest levels of *Il17a*
216 (**Fig. 4B and Table S4**), while cluster c6 was contaminated with αβ T cells (**Fig. 4B and Table**
217 **S4**). Clusters c2 and c4 had distinct proliferative signatures (**Fig. 4B and Table S4**) and showed
218 increased abundance in EAE, however, considerably more in Cre$^+$ mice (**Fig. 4C**). Interestingly,
219 cluster c1 expressed a number of IFN-induced genes (e.g. *Nkg7*, *Irf7*, *Gbp6*, *Zbp1*) together with
220 *Tbx21*, downregulated *Ccr6* and was the cluster whose abundance increased after EAE and only
221 in Cre$^-$ mice (**Fig. 4B-D**). Additionally, cluster c1 had detectable *Ifng* and reduced levels of *Il17a*
222 compared to other clusters (**Fig. 4B, D**).
223 Analysis of DEGs showed that at d0, Cre$^+$ cells had a clear reduction in genes involved in
224 TCR, cytokine and NF-κB signaling (e.g. *Jun*, *Fos*, *Nr4a1*, *Tnfaip3*, *Itk*) (**Fig. 4E and Table S5**),
225 suggesting that when RARα is inactive Vγ4$^+$ γδT17 cells have impaired propensity to become
226 activated. As such, at d11, it was mostly Cre$^-$ cells that upregulated genes classically associated
227 with activated T cells and IFN signaling such as *Ctla4*, *Ly6a*, *Stat4*, and *Zbp1*, in addition to the
228 cytokine *Csf2* and the pro-survival GIMAP genes *Gimap5*, *Gimap6*, and *Gimap8* together with *Bcl3*
229 (**Fig. 4E and Table S5**). In contrast, genes that discerned Cre$^+$ cells responding to immunization
230 included the adhesion molecules *Ccr10* and *Itgae*, *Il21r*, and *Tnf* (**Fig. 4E and Table S5**). We did
231 not find any proliferation or cell cycle related genes that were downregulated in Cre$^+$ cells
232 suggesting intact proliferative capacity (**Table S5**). Collectively, these data show that RARα

233 maintains a status of activation and survival without interfering with cell proliferation, and that
234 during EAE supports Vγ4$^+$Vδ2-2$^+$ γδT17 cells characterized by an IFN gene signature.
235 When we investigated Vγ6$^+$ cells, we identified 6 clusters, all with a type 3 identity, of which c4
236 was a *Scart2*$^+$ contaminant (**Fig. S3A-B and Table S4**). Cluster c1 expressed higher levels of
237 *Egr1*, and was nearly absent in Cre$^+$ cells prior to immunization (**Fig. S3B-C and Table S4**).
238 Cluster c2 could be distinguished by high levels of *Tnfsf11* and *Stab2* as well as lower *Il17a*, and
239 both before and after immunization was more prevalent in Cre$^+$ cells (**Fig. S3B-C and Table S4**).
240 Cluster c3, similar to Vγ4$^+$ cluster c1, downregulated *Ccr6*, expressed *Tbx21* and had a distinct IFN
241 signature (**Fig. S3B and Table S4**). As was the case for the Vγ4$^+$ counterpart, this cluster had
242 reduced levels of *Il17a* and detectable transcripts of *Ifng* and although its abundance did not
243 increase in EAE, it was more prevalent in Cre$^-$ cells (**Fig. S3B-D**). Cluster c5 was of very low
244 frequency, had a proliferation related gene signature and was more abundant at d11 after EAE
245 induction in Cre$^+$ mice (**Fig. S3C**). Cre$^-$ Vγ6$^+$ cells appeared to be relatively unresponsive to EAE,
246 with the exception of a modest increase observed for cluster c0 (**Fig. S3C**), while the abundance of
247 cluster c1 was much higher in Cre$^+$ cells after immunization (**Fig. S3C**).
248 Analysis of DEGs among genotypes and time points revealed transcriptional changes
249 relatively similar to Vγ4$^+$ cells (**Table S5**). Thus, at d0, Cre$^-$ cells had high expression of many
250 genes related to immune signaling pathways (e.g. *Nr4a1*, *Dusp2*, *Rel*), immune cell activation (e.g.
251 *Il17a*, *Cd69*, *Itga4*) and survival (*Gimap8*, *Gimap9*, *Bcl2a1d*), indicating a better cellular fitness
252 during immune responses (**Fig. S3E and Table S5**). A lot of these genes were downregulated at
253 d11 of EAE and a fraction was now more highly expressed in Cre$^+$ cells (**Fig. S3E and Table S5**).
254 Instead, Cre$^-$ Vγ6$^+$ cells showed induction of IFN-associated genes after immunization (e.g. *Ly6a*,
255 *Ifi47*, *Stat4*) (**Fig. S3E and Table S5**). These data suggest that Vγ6$^+$ cells with active RARα are
256 better equipped to survive and react to inflammatory stimuli, they too show an IFN gene signature,
257 however, they do not respond well to EAE.
258
259 **RA is necessary for EAE mediated neuroinflammation**
260 The above data suggested that γδT17 cells with inactive RARα would be defective in mounting a
261 response during EAE. To test this, we immunized mice and analyzed cell numbers and cytokine

262 production in the spleen. We found that at d11 post immunization, there was a dramatic reduction
263 in the numbers of Cre$^+$ Vγ4$^+$ cells (**Fig. 5A**). While the number of normal Vγ4$^+$ γδT17 cells
264 increased on average 19-fold by d11, their Cre$^+$ counterparts increased 9-fold (**Fig. 5A**). At the
265 same time, there was a profound loss of IL-17A-producing cells (**Fig. 5B and Fig. S4A**). To correct
266 for the highly reduced numbers of Cre$^+$ cells, we assessed the frequency of IL-17A$^+$ cells within the
267 Vγ4$^+$ γδT17 population. We found that Cre$^+$ Vγ4$^+$ γδT17 cells were compromised in their ability to
268 produce IL-17A (**Fig. 5C**). The EAE-induced increase of Vγ4$^-$ γδT17 cell numbers was
269 considerably less prominent, and the impact of RARα was insignificant (**Fig. S4B**), which agreed
270 with our scRNA-seq data (**Fig. S3C**). We additionally observed that Vγ4$^+$ cells could produce low
271 amounts of IFN-γ together with IL-17A and this was RA-dependent (**Fig. 5D-E**). This may
272 represent the type 1 *Ifng*-expressing c1 cluster in our scRNA-seq dataset (**Fig. 4C-D**). Although we
273 had observed a similar cluster (c3) in Vγ4$^-$ cells (**Fig. S3C-D**), we could not detect IFN-γ protein by
274 flow cytometry (**Fig. S4C-D**). By d21 post immunization, the γδT17 response had subsided (**Fig.
275 5A** and **Fig. S4B**). Concomitantly, we found that Cre$^+$ mice developed significantly reduced
276 paralysis symptoms (**Fig. 5F**) and retained their body weight (**Fig. 5G**). This profound resilience to
277 developing EAE disease was puzzling, since mice deficient in all γδ T cells have delayed disease
278 but still develop evident symptoms (*51*). We thus hypothesized that the phenotype of RORγt^{CRE}-
279 RARdn$^{F/F}$ mice could be explained by an additional defect in T_H17 cells, which are necessary for
280 EAE pathogenesis (*52*), and which get help from γδT17 cells (*50, 51*). In this regard, we found
281 defects in the CD4$^+$ T cell compartment at d11 of EAE, coinciding with the defective γδT17
282 response. Hence, although numbers of activated CD44$^+$CD4$^+$ T cells were only slightly reduced at
283 d11 (**Fig. S4E**), there was a significant impairment in their ability to produce IL-17A and IFN-γ (**Fig.
284 S4F-I**). Thus, RA is important for the full development of EAE-associated symptoms and for Vγ4$^+$
285 γδT17 and T_H17 cells to efficiently respond to neuroinflammatory stimuli.
286
287 **RA is required for α4β1 expression and γδT17 cell infiltration to the brain**
288 A key role of RA in the immune system is the imprinting of the gut homing molecules CCR9 and
289 α4β7 on T cells (*17*). We had also observed that RA regulated genes related to cell adhesion and
290 migration in thymic γδT17 cells (**Fig. 1 and Table S2**). Thus, we examined the DEGs between

291 Cre$^+$ and Cre$^-$ Vγ4$^+$ γδT17 cells at d11 of EAE and identified transcripts related to cell adhesion,
292 migration or tissue retention (**Table S6**). We identified 19 such genes, 4 of which were higher and
293 8 were lower in Cre$^+$ cells at d11, while 7 remained unchanged (**Fig. 6A**). Differences included the
294 downregulation of *Rasa3*, important for T cell entry and exit from SLOs but also T cell responses
295 and T_H17 pathology during EAE (*53, 54*), and the upregulation of *Rgs1*, which negatively regulates
296 chemokine receptor signaling (*55*) (**Fig. 6A**). Notably, *Itgb1*, which codes the β1 integrin chain, was
297 also significantly downregulated in Cre$^+$ cells (**Fig. 6A**). The β1 can pair with the α4 chain to form
298 the α4β1 integrin, also known as VLA-4 (*56, 57*), which is important for the homing of pathogenic
299 lymphocytes to the brain during EAE and has been used as a therapeutic target in multiple
300 sclerosis (MS) (*58-60*). We therefore wanted to test whether levels of α4β1 are altered in cells with
301 inactive RARα. To do this, we co-stained with antibodies that mark the α4β7 complex, and either
302 the α4 or β1 chains at d0 and d11 of EAE. Hence, by gating out α4β7$^+$ cells and focusing on cells
303 co-expressing the α4 and β1 chains, we could discern α4β1$^+$ cells. We found that γδT17 cells
304 expressed significantly less α4β1 when RARα was inactive (**Fig. 6B-C**), and of the α4β1-
305 expressing γδT17 population over 80% were Vγ4$^+$ (**Fig. 6D**). Reduced expression of α4β1 was
306 also evident in CD44$^+$CD4$^+$ T cells (**Fig. S5A-B**). Failed induction of surface α4β1 correlated with
307 impaired γδT17 and CD44$^+$CD4$^+$ T cell infiltration into the brain (**Fig. 6E and Fig. S5C**). Although
308 the low cell numbers in the brain might simply reflect the low numbers of responding cells in the
309 periphery, it helps to further explain the profound resistance of RORγt^{CRE}-RARdn$^{F/F}$ mice to EAE.
310

311 **Discussion**

312 In the present study we demonstrate that RA and its nuclear receptor RARα act on multiple levels
313 to regulate the development, homeostasis and inflammatory responses of IL-17-producing γδ T
314 cells. We found that cells unable to sense RA through RARα in the embryonic and newborn
315 thymus undergo a transcriptional reorganization affecting a multitude of signaling modalities,
316 homing and tissue retention potential in addition to survival. As such, our data suggest that RA
317 strengthens TCR signaling in the embryonic thymus putting thus a break on γδT17 development,
318 while after birth RA is critical to maintain survival of newly developed cells by counteracting
319 apoptosis. In adult mice and during the course of EAE neuroinflammation, RA sustains a
320 transcriptional program that indicates high propensity to respond to inflammatory stimuli and
321 immunization, especially in Vγ4^{+} γδT17 cells. Thus, Vγ4^{+} γδT17 cells with inactive RARα failed to
322 sufficiently increase in numbers or produce cytokines in response to EAE. This was accompanied
323 by reduced expression of the integrin α4β1 and accumulation of cells in the brain. Consequently,
324 and combined with a defective effector CD4^{+} T cell compartment, RORγt^{CRE}-RARdn$^{F/F}$ mice were
325 almost resistant to EAE associated symptoms.

326 It is well-established that the strength of the TCR during thymic development is an important
327 determinant for the lineage choices of γδ T cells. The current model suggests that cells who
328 escape Skint-1 selection and do not become Vγ5^{+}, receive either strong or weak TCR signals, the
329 latter of which, through the PI3K-Akt pathway, determine their ability to become γδT17 (*5-7, 48*). In
330 contrast, strong ERK-dependent TCR signals promote the generation of IFN-γ-producing γδT1
331 cells (*6*). Although Vγ4^{+} γδT17 appear less dependent on the TCR and are generated from pre-
332 programmed Sox13^{+} DN1d progenitors, they too need TCR signaling to transition to fully mature
333 IL-17-producing cells (*61*). Our data show that inactivation or inhibition of RARα reduces the TCR
334 signaling strength, favoring thus the generation of γδT17 cells in the embryonic and newborn
335 thymus. It is most likely that this is regulated at the gene expression level, since we found that cells
336 with inactive RARα have impaired transcriptional modalities related to TCR, especially in
337 embryonic life. Thus, gene expression and hence biological effects downstream of the TCR are
338 impaired in the absence of RARα or RA sensing. Previous data in conventional T cells have also
339 showed that RARα may cooperate with TCR mobilized transcription factors, such as NFATc2, to

340 induce gene expression (*62*), suggesting a broader role of RA in fine tuning the outcome of TCR
341 signaling. Recently, a novel RARα isoform located in the cytoplasm was shown to interact directly
342 with the αβTCR and Zap70 to strengthen early signaling (*63*). Although there is no evidence that
343 this isoform is relevant or expressed in γδ T cells, RARα inhibition in our FTOC experiments could
344 have interfered with both nuclear and cytoplasmic RARα. This notwithstanding, RA and its
345 interaction with RARα comprise a mechanism by which the strength of the γδTCR can be fine-
346 tuned to balance lineage choice of developing γδ T cell subsets.
347 Besides TCR signaling, thymic γδ T cells that could not sense RA downregulated many genes
348 related to T cell activation, adhesion, migration, tissue retention and survival. This was not
349 surprising as RA and its nuclear receptors regulate thousands of genes in multiple cell types and
350 tissues throughout life. Notably, there were many genes downregulated, especially in newborn
351 γδT17 cells, related to survival, including *Bcl2* and a number of GIMAP transcripts, which led to
352 increased levels of apoptosis. RA is a well-known regulator of cell death and survival, and although
353 it has been shown to possess both pro- and anti-apoptotic activity, it is mostly considered as an
354 inducer of apoptosis (*64*). However, RA can prevent apoptotic death in cardiomyocytes (*65*) as well
355 as in developing brain cells (*44*), while early studies in T cells had suggested that RA could inhibit
356 activation induced cell death (*66, 67*). Although the mechanisms by which RA may inhibit
357 apoptosis in T cells have not been discerned, it is plausible that they are transcriptionally regulated
358 through direct or indirect induction of genes that enhance survival and counteract cell death.
359 GIMAP genes for example have been shown to be transcriptional targets of RARα (*36*). It is also
360 plausible that the survival defects that we observed in RARα inactive cells could be due to
361 continuous weak TCR signaling, evident by the partial rescue of Bcl-2 in α-CD3 stimulated
362 newborn γδT17 cells. In this regard, continuous weakening of the TCR signal will eventually result
363 in the deletion of developing γδT17 cells (*48*). However, it is not yet known whether the γδTCR is
364 actively signaling in the periphery and whether this is required to sustain homeostatic survival.
365 Collectively, the data suggest that through direct transcriptional targeting and by strengthening the
366 γδTCR signal, RA and RARα impact in unison, and/or sequentially, thymic development and
367 extrathymic survival of γδT17 cells.

368 T_H17 and γδT17 cells are the major pathogenic populations in EAE (*51, 52, 68*) and their
369 presence in MS has been correlated with disease severity (*69-72*). Hence, suppressing IL-17-
370 secreting T cells could be beneficial in limiting MS pathology (*73-75*). Our data reveal that inability
371 to sense RA reduces the propensity of γδT17 cells to become activated by regulating multiple
372 transcriptional programs, including those associated with response to IFNs, survival, cytokine
373 production and homing to the brain. The observation that IFN genes were readily inducible and
374 RA-dependent, and that type 1-like γδT17 cells were highly abundant in EAE is reminiscent of T_H
375 responses, which convert from type 3 to type 1 during disease progression (*76, 77*). Whether
376 sensing of IFN or production of IFN-γ makes γδT17 subsets more pathogenic in EAE or it simply
377 denotes activated cells has not been tested. Nevertheless, RORγt-Cre-mediated impairment of RA
378 sensing led to a profound resistance in EAE disease. The data suggest that this was not only due
379 to the aforementioned defects in γδT17 cells, but that parallel defects in T_H17 cells contributed. In
380 our transgenic model, RORγt$^+$ type 3 cells develop in an "RA-less" environment, which we believe
381 destabilizes them over time and become functionally incompetent. This raises the hypothesis that
382 continuous exposure to low or high levels of dietary vitamin A from embryogenesis and neonatal to
383 adult life may modulate fundamental transcriptional programs in type 3 cells impacting on their
384 ability to mount immune responses. Thus, acutely altering the concentrations of available RA in
385 competent cells may have very different outcomes. In this regard, administration of RA during
386 ongoing EAE or pre-treatment of donor cells with RA prior to transfer into recipient mice
387 suppressed the function of both T_H17 and γδT17 cells and reduced disease severity (*41, 78*).
388 Consequently, despite the importance of RA in arming type 3 effector T cell populations during
389 development and maturation, sudden exposure to high concentrations of RA may have the
390 opposite effects.
391 Collectively, the data presented herein suggest that RA impacts γδ T cells from embryonic to
392 neonatal to adult life and during inflammatory responses, and ensures their normal development,
393 their survival and their ability to participate in immune responses. It would be of interest to explore
394 whether low or high levels of dietary intake of vitamin A during pregnancy and infancy are able to
395 modulate the biology of γδ T and other immune cells.
396

Acknowledgments

We would like to thank everyone at the BioFacility at the Technical University of Denmark for continuous support with animal studies. The study was funded by the Lundbeck Foundation (R366-2021-104) and the Novo Nordisk Foundation (NNF24OC0095974). NS and DP were funded by the BBSRC (BB/R017808/1).

Author contributions

VB conceived the study, wrote the manuscript and analyzed data. MGFFdS and RA performed the experiments, analyzed the data and helped write the manuscript. JR, JF, ECF, MVB, DS and PPS helped with experiments, NS and DP performed all experiments related to FTOCs and helped write the manuscript.

409 **Materials and Methods**

410 **Mice**

411 All animal breeding and experiments were performed in-house at the BioFacility within the
412 Technical University of Denmark and only after approval from the Danish Animal Experiments
413 Inspectorate or at Queen Mary University of London in full compliance with UK Home Office
414 guidelines. RORγt^{CRE} and *Rorc(γt)-Gfp*^{TG} reporter (RORγt-GFP$^{+/-}$) (*43*) mice were provided by
415 Gerard Eberl. RARdn$^{F/F}$ mice (*44*) were provided by William Agace after permission from San
416 Sockanathan.

417

418 **Cell preparation and culture**

419 Dissected adult, embryonic, newborn and neonatal lymphoid organs were isolated and crushed
420 through a cell strainer and washed before being re-suspended in culture media (RPMI containing
421 10% FBS, Penicillin/Streptomycin, 0.1% β-ME, 20 mM HEPES and L-Glutamine) (ThermoFisher).
422 An extra RBC lysis step was used for spleens. To isolate lymphocytes from the brain, mice were
423 euthanized by CO_2 asphyxiation, perfused with cold PBS and the whole brain was additionally
424 rinsed in PBS. The tissue was cut in smaller pieces and digested for 30 minutes at 37 ºC with 10
425 mg/ml DNase I (Sigma-Aldrich) and 10 mg/mL type IV collagenase from *Clostridium histolyticum*
426 (Sigma-Aldrich), pipetting up and down every 10 minutes. Afterwards, the remaining tissue was
427 homogenized with a Pasteur pipette and crushed through a cell strainer. Lymphocytes were
428 separated using density gradient centrifugation with 37% Percoll (GE Healthcare) layered on 70%
429 Percoll and centrifuged at 20 °C and 900 × *g* for 30 min with deceleration set to 0. Cells from the
430 interphase were collected and washed once before used for staining. Cells from lymphoid organs
431 were counted using a Sysmex XP-300. Cell counts from brain were determined using
432 CountBright™ Absolute Counting Beads (ThermoFisher).

433

434 ***Ex vivo* culturing of lymphocytes**

435 For cytokine detection cells were cultured for 3.5 hours in the presence of 50 ng/ml PMA (Sigma-
436 Aldrich, 750 ng/ml Ionomycin (Sigma-Aldrich) and 1 µl/ml BD GolgiStop (containing monensin). For
437 determination of Bcl-2 levels after TCR stimulation, newborn thymocytes (isolated as described

438 above) were cultured with or without 1 μg/ml soluble α-CD3 (clone 145-2C11, BioXCell) overnight
439 (16 h). To measure the degree of apoptosis, the CellEvent Caspase-3/7 Green Flow Cytometry
440 Assay Kit (Invitrogen) was used. In short, newborn thymocytes were cultured for 40h in culture
441 media and 1 μl/ml of detection reagent was added 30 minutes before harvesting. In all cases, cells
442 were incubated at 37ºC, harvested and used for flow cytometry staining.
443
444 **Fetal thymic organ cultures (FTOCs)**
445 Embryonic e15 thymic lobes from time-mated C57BL/6 or RORγt-GFP$^{+/-}$ mice were cultured on
446 nucleopore membrane filter discs (Whatman) in culture media (RPMI with 10% heat-inactivated
447 FBS, Penicillin/Streptomycin, 0.1% β-ME, and L-Glutamine) (all reagents from ThermoFisher) for 7
448 days under control conditions or in the presence of either 160 nM ATRA (Sigma-Aldrich) or 2 or 8
449 μM of the selective RARα antagonist Ro 41-5253 (Sigma-Aldrich). In cultures containing Ro41,
450 anti-TCRδ antibody GL3 (ThermoFisher) was added at a concentration of 0.5 μg/ml. All cultures
451 were rested overnight in fresh media before analysis by flow cytometry.
452
453 **Experimental Autoimmune Encephalomyelitis**
454 EAE was induced by sub-cutaneous injection of 50 μg of MOG_{35-55} peptide in CFA, while 200 ng
455 pertussis toxin were injected intra-peritoneally (i.p.) on the day of immunization and 2 days later.
456 From day 11 after immunization and until day 21, mice were weighed and scored for clinical signs
457 as follows: 0: no symptoms; 1: tail paralysis; 1.5: impaired righting reflex; 2: paralysis of one hind
458 limb; 2.5: paralysis of both hind limbs; 3: paralysis of one fore limb; 3.5: paralysis of one fore limb
459 and weak second limb; 4: total limb paralysis. Mice were euthanized at day 21 after immunization.
460 Lymphocytes from the brain and lymphoid organs were isolated as described above.
461
462 **Flow Cytometry**
463 Cells were stained in U-bottom 96-well plates in 75 μl PBS containing 3% FBS with combinations
464 of the following antibodies: CD4-FITC (RM4-4), CD19-FITC (6D5; Biolegend), CD8α-FITC (53-6.7),
465 Vγ4-PerCP-eF710 (UC3-10A6; ThermoFisher), CD11b-PerCP-Cy5.5 (M1/70), IFNγ-APC
466 (XMG1.2; BioLegend), CD29-APC (eBioHMb1-1; ThermoFisher), Vγ1-APC (2.11; Biolegend),

467 CCR6-AF647 (140706), TCRβ-APCeF780 (H57-597; ThermoFisher), CD45RB-PE (16A), IFNγ-PE
468 (XMG1.2; BioLegend), CD49d-PE (R1-2; ThermoFisher), Vγ4-PE (UC3-10A6; Biolegend); Bcl2-PE
469 (BCL/10C4; Biolegend), α4β7-PECF594 (DATK32), CD3-PECF594 (145-2C11), CD24-PECy7
470 (M1/69), CD27-PECy7 (LG.3A10), CD73-PECy7 (BioTY/11.8; ThermoFisher), IFNγ-APC
471 (XMG1.2), CD3-PECy7 (145-2C11), CD3-PE (145-2C11; BioLegend), RORγt-APC (B2D), TCRγδ-
472 BV421 (GL3), CD44-V500 (IM7), CD45-V500 (30-F11), CD45.2-BV650 (104; Biolegend), CD27-
473 BV650 (LG.3A10), IL-17A-BV786 (TC11-18H10), CD8α-BV786 (53-6.7), CD45-BUV395 (I3/2.3),
474 CD19-Alexa Fluor 700 (1D3). Cells were stained for 30 minutes on ice and all antibodies were
475 used at a 1:200 dilution. Prior to antibody staining, cells were incubated on ice with 100 µl of
476 Fixable Viability Dye AF700 at a 1:1000 dilution in PBS. Cells were washed in 150 µl PBS
477 containing 3% FBS in-between steps. Intracellular cytokine and transcription factor staining was
478 performed using the eBioscience FoxP3 Transcription Factor Staining kit (ThermoFisher)
479 according to the manufacturer's instructions. Unless specified all antibodies and staining reagents
480 were purchased from BD Biosciences. Samples were acquired on a BD LSR Fortessa using BD
481 FACSDiva software v8.0.2. For sorting, the staining was carried out as described above but using
482 PBS containing 0.5% BSA instead, and cells were sorted on BD FACSAria III.
483
484 **Single-cell RNA-seq**
485 Thymic and splenic cells were prepared and stained as described above for cell sorting. However,
486 cells were first incubated with 0.25 µg TruStain FcX PLUS (Biolegend) for 10 minutes on ice.
487 Without washing in between, cells from each mouse litter (3 for each timepoint) were hashed for 30
488 minutes on ice with TotalSeq-C0304, TotalSeq-C0305 and TotalSeq-C0306 antibodies (1 µg per
489 10^6 cells) (Biolegend) respectively. For e18, only one litter was used. Afterwards, the antibody
490 cocktail combined with the viability dye was directly added without a washing step and left for 30
491 minutes. Cells were then washed 3 times and sorted based on the gating strategy depicted in
492 Figure S1A. Following the 10X Genomics Single Cell 5' Chemistry (v2) platform, sorted γδT17 cells
493 were loaded into a Chromium Controller and processed according to the manufacturer's
494 instructions. Library quality control and quantification were done using a 2100 Bioanalyzer
495 equipped with a High Sensitivity DNA kit (Agilent, 5067-4626). Libraries were pooled and

496 sequenced on a NovaSeq 6000 instrument at the Flow Cytometry & Single Cell Core Facility at the
497 University of Copenhagen, Denmark.
498
499 **Data Analysis**
500 Flow cytometry data was analyzed using Flow Jo v9.8.3 or v10. In lymphoid organs, γδT17 cells
501 were gated as depicted in Figure S1A and in the brain they were identified as
502 $CD11b^{-}CD45^{+}CD3^{+}CD4^{-}TCR\beta^{-}TCR\gamma\delta^{+}CD44^{+}CD27^{-}$. All graphs not depicting single-cell data were
503 generated and analyzed using Prism v8 or v10. Details for statistical tests are shown in each
504 individual figure legend. For the scRNA-seq data, sequencing quality control and demultiplexing
505 was carried out by the Flow Cytometry & Single Cell Core Facility at the University of Copenhagen.
506 Reads were filtered and aligned to the GRCm39-2024-A reference genome using CellRanger
507 v8.0.0. Seurat v5.1.0 was used for additional quality control and data analysis. Datasets were
508 preprocessed individually; HTODemux was used to demultiplex hashed biological replicates,
509 remove doublets and non-labeled cells. Cells with more than 5% mitochondrial counts and
510 aberrantly low or high number of RNA molecules and genes were also excluded. In addition,
511 ribosomal genes were removed. Afterwards, datasets were merged (e18 with newborn thymus; d0
512 control with d11 EAE spleen). The data was Log Normalized, and the effect of cell cycle variance
513 was regressed out. Thymic and splenic datasets were integrated separately using Canonical
514 Correlation Analysis (CCA). In the EAE data, we found contaminating myeloid cells (identified
515 based on *Spi1*) and other non-T cells based on lack of *Cd3e* expression, and these were removed
516 from the pool of cells. Then, Vγ4 and Vγ6 cells were subsetted based on the condition that cells
517 express at least one transcript of *Trgv4* or *Trgv6*, respectively, and do not express any transcripts
518 from the other chain. After subsetting, the data was re-scaled and re-integrated. Afterwards,
519 unsupervised clustering was run with default parameters for the thymus, spleen Vγ4 and Vγ6
520 datasets. Cluster identities were found running Seurat´s “FindAllMarkers” function. Differential
521 expression analysis was done using “FindMarkers”. In all cases, only genes expressed in at least
522 25% of cells and with a $\log_2$FC of ≥ 1 and an adjusted p-value of <0.05 (determined using a
523 Wilcoxon Rank Sum test) were considered significant.
524

References

1. E. S. Edholm, M. Banach, J. Robert, Evolution of innate-like T cells and their selection by MHC class I-like molecules. *Immunogenetics* **68**, 525-536 (2016).
2. M. Hirano *et al.*, Evolutionary implications of a third lymphocyte lineage in lampreys. *Nature* **501**, 435-438 (2013).
3. R. Agerholm, V. Bekiaris, Evolved to protect, designed to destroy: IL-17-producing gammadelta T cells in infection, inflammation, and cancer. *Eur J Immunol*, (2021).
4. J. C. Ribot *et al.*, CD27 is a thymic determinant of the balance between interferon-gamma- and interleukin 17-producing gammadelta T cell subsets. *Nat Immunol* **10**, 427-436 (2009).
5. G. Turchinovich, A. C. Hayday, Skint-1 identifies a common molecular mechanism for the development of interferon-gamma-secreting versus interleukin-17-secreting gammadelta T cells. *Immunity* **35**, 59-68 (2011).
6. N. Sumaria, C. L. Grandjean, B. Silva-Santos, D. J. Pennington, Strong TCRgammadelta Signaling Prohibits Thymic Development of IL-17A-Secreting gammadelta T Cells. *Cell reports* **19**, 2469-2476 (2017).
7. M. Munoz-Ruiz *et al.*, TCR signal strength controls thymic differentiation of discrete proinflammatory gammadelta T cell subsets. *Nat Immunol* **17**, 721-727 (2016).
8. M. K. Zuberbuehler *et al.*, The transcription factor c-Maf is essential for the commitment of IL-17-producing gammadelta T cells. *Nat Immunol* **20**, 73-85 (2019).
9. I. Prinz, B. Silva-Santos, D. J. Pennington, Functional development of gammadelta T cells. *Eur J Immunol* **43**, 1988-1994 (2013).
10. D. Kadekar *et al.*, The neonatal microenvironment programs innate gammadelta T cells through the transcription factor STAT5. *J Clin Invest* **130**, 2496-2508 (2020).
11. J. Rizk *et al.*, The cIAP ubiquitin ligases sustain type 3 gammadelta T cells and ILC during aging to promote barrier immunity. *J Exp Med* **220**, (2023).
12. B. S. Sheridan *et al.*, gammadelta T cells exhibit multifunctional and protective memory in intestinal tissues. *Immunity* **39**, 184-195 (2013).
13. A. C. Kohlgruber *et al.*, gammadelta T cells producing interleukin-17A regulate adipose regulatory T cell homeostasis and thermogenesis. *Nat Immunol* **19**, 464-474 (2018).
14. A. O. Mann *et al.*, IL-17A-producing gammadeltaT cells promote muscle regeneration in a microbiota-dependent manner. *J Exp Med* **219**, (2022).
15. M. Ribeiro *et al.*, Meningeal gammadelta T cell-derived IL-17 controls synaptic plasticity and short-term memory. *Sci Immunol* **4**, (2019).
16. K. Alves de Lima *et al.*, Meningeal gammadelta T cells regulate anxiety-like behavior via IL-17a signaling in neurons. *Nat Immunol* **21**, 1421-1429 (2020).
17. M. N. Erkelens, R. E. Mebius, Retinoic Acid and Immune Homeostasis: A Balancing Act. *Trends Immunol* **38**, 168-180 (2017).
18. D. N. D'Ambrosio, R. D. Clugston, W. S. Blaner, Vitamin A metabolism: an update. *Nutrients* **3**, 63-103 (2011).
19. J. S. Steinhoff, A. Lass, M. Schupp, Biological Functions of RBP4 and Its Relevance for Human Diseases. *Front Physiol* **12**, 659977 (2021).
20. N. B. Ghyselinck, G. Duester, Retinoic acid signaling pathways. *Development* **146**, (2019).
21. J. A. Hall, J. R. Grainger, S. P. Spencer, Y. Belkaid, The role of retinoic acid in tolerance and immunity. *Immunity* **35**, 13-22 (2011).
22. G. Duester, Retinoic acid synthesis and signaling during early organogenesis. *Cell* **134**, 921-931 (2008).
23. C. O'Connor, P. Varshosaz, A. R. Moise, Mechanisms of Feedback Regulation of Vitamin A Metabolism. *Nutrients* **14**, (2022).

575 24. M. R. Conserva, L. Anelli, A. Zagaria, G. Specchia, F. Albano, The Pleiotropic Role of
576 Retinoic Acid/Retinoic Acid Receptors Signaling: From Vitamin A Metabolism to Gene
577 Rearrangements in Acute Promyelocytic Leukemia. *Int J Mol Sci* **20**, (2019).
578 25. N. R. de Almeida, M. Conda-Sheridan, A review of the molecular design and biological
579 activities of RXR agonists. *Med Res Rev* **39**, 1372-1397 (2019).
580 26. S. A. van de Pavert *et al.*, Chemokine CXCL13 is essential for lymph node initiation and
581 is induced by retinoic acid and neuronal stimulation. *Nat Immunol* **10**, 1193-1199
582 (2009).
583 27. S. A. van de Pavert *et al.*, Maternal retinoids control type 3 innate lymphoid cells and
584 set the offspring immunity. *Nature* **508**, 123-127 (2014).
585 28. W. W. Agace, E. K. Persson, How vitamin A metabolizing dendritic cells are generated in
586 the gut mucosa. *Trends Immunol* **33**, 42-48 (2012).
587 29. K. M. Luda *et al.*, IRF8 Transcription-Factor-Dependent Classical Dendritic Cells Are
588 Essential for Intestinal T Cell Homeostasis. *Immunity* **44**, 860-874 (2016).
589 30. M. H. Kim, E. J. Taparowsky, C. H. Kim, Retinoic Acid Differentially Regulates the
590 Migration of Innate Lymphoid Cell Subsets to the Gut. *Immunity* **43**, 107-119 (2015).
591 31. J. L. Coombes *et al.*, A functionally specialized population of mucosal CD103+ DCs
592 induces Foxp3+ regulatory T cells via a TGF-beta and retinoic acid-dependent
593 mechanism. *J Exp Med* **204**, 1757-1764 (2007).
594 32. C. M. Sun *et al.*, Small intestine lamina propria dendritic cells promote de novo
595 generation of Foxp3 T reg cells via retinoic acid. *J Exp Med* **204**, 1775-1785 (2007).
596 33. D. Mucida *et al.*, Reciprocal TH17 and regulatory T cell differentiation mediated by
597 retinoic acid. *Science* **317**, 256-260 (2007).
598 34. H. R. Cha *et al.*, Downregulation of Th17 cells in the small intestine by disruption of gut
599 flora in the absence of retinoic acid. *J Immunol* **184**, 6799-6806 (2010).
600 35. J. A. Hall *et al.*, Essential role for retinoic acid in the promotion of CD4(+) T cell effector
601 responses via retinoic acid receptor alpha. *Immunity* **34**, 435-447 (2011).
602 36. C. C. Brown *et al.*, Retinoic acid is essential for Th1 cell lineage stability and prevents
603 transition to a Th17 cell program. *Immunity* **42**, 499-511 (2015).
604 37. B. S. Reis, D. P. Hoytema van Konijnenburg, S. I. Grivennikov, D. Mucida, Transcription
605 factor T-bet regulates intraepithelial lymphocyte functional maturation. *Immunity* **41**,
606 244-256 (2014).
607 38. B. S. Reis, A. Rogoz, F. A. Costa-Pinto, I. Taniuchi, D. Mucida, Mutual expression of the
608 transcription factors Runx3 and ThPOK regulates intestinal CD4(+) T cell immunity.
609 *Nat Immunol* **14**, 271-280 (2013).
610 39. A. Obers *et al.*, Retinoic acid and TGF-beta orchestrate organ-specific programs of
611 tissue residency. *Immunity* **57**, 2615-2633 e2610 (2024).
612 40. Z. Qiu *et al.*, Retinoic acid signaling during priming licenses intestinal CD103+ CD8
613 TRM cell differentiation. *J Exp Med* **220**, (2023).
614 41. M. Raverdeau, C. J. Breen, A. Misiak, K. H. Mills, Retinoic acid suppresses IL-17
615 production and pathogenic activity of gammadelta T cells in CNS autoimmunity.
616 *Immunol Cell Biol* **94**, 763-773 (2016).
617 42. L. A. Mielke *et al.*, Retinoic acid expression associates with enhanced IL-22 production
618 by gammadelta T cells and innate lymphoid cells and attenuation of intestinal
619 inflammation. *J Exp Med* **210**, 1117-1124 (2013).
620 43. M. Lochner *et al.*, In vivo equilibrium of proinflammatory IL-17+ and regulatory IL-10+
621 Foxp3+ RORgamma t+ T cells. *J Exp Med* **205**, 1381-1393 (2008).
622 44. F. Rajaii, Z. T. Bitzer, Q. Xu, S. Sockanathan, Expression of the dominant negative
623 retinoid receptor, RAR403, alters telencephalic progenitor proliferation, survival, and
624 cell fate specification. *Dev Biol* **316**, 371-382 (2008).

45. J. S. Heilig, S. Tonegawa, Diversity of murine gamma genes and expression in fetal and adult T lymphocytes. *Nature* **322**, 836-840 (1986).
46. C. M. Carlson *et al.*, Kruppel-like factor 2 regulates thymocyte and T-cell migration. *Nature* **442**, 299-302 (2006).
47. S. Filen, R. Lahesmaa, GIMAP Proteins in T-Lymphocytes. *J Signal Transduct* **2010**, 268589 (2010).
48. N. Sumaria, S. Martin, D. J. Pennington, Constrained TCRgammadelta-associated Syk activity engages PI3K to facilitate thymic development of IL-17A-secreting gammadelta T cells. *Sci Signal* **14**, (2021).
49. F. Coffey *et al.*, The TCR ligand-inducible expression of CD73 marks gammadelta lineage commitment and a metastable intermediate in effector specification. *J Exp Med* **211**, 329-343 (2014).
50. A. M. McGinley *et al.*, Interleukin-17A Serves a Priming Role in Autoimmunity by Recruiting IL-1beta-Producing Myeloid Cells that Promote Pathogenic T Cells. *Immunity* **52**, 342-356 e346 (2020).
51. C. E. Sutton *et al.*, Interleukin-1 and IL-23 induce innate IL-17 production from gammadelta T cells, amplifying Th17 responses and autoimmunity. *Immunity* **31**, 331-341 (2009).
52. Ivanov, II *et al.*, The orphan nuclear receptor RORgammat directs the differentiation program of proinflammatory IL-17+ T helper cells. *Cell* **126**, 1121-1133 (2006).
53. K. H. Johansen *et al.*, A CRISPR screen targeting PI3K effectors identifies RASA3 as a negative regulator of LFA-1-mediated adhesion in T cells. *Sci Signal* **15**, eabl9169 (2022).
54. B. Wu *et al.*, RAS P21 Protein Activator 3 (RASA3) Specifically Promotes Pathogenic T Helper 17 Cell Generation by Repressing T-Helper-2-Cell-Biased Programs. *Immunity* **49**, 886-898 e885 (2018).
55. E. P. Bowman *et al.*, Regulation of chemotactic and proadhesive responses to chemoattractant receptors by RGS (regulator of G-protein signaling) family members. *J Biol Chem* **273**, 28040-28048 (1998).
56. K. G. Haanstra *et al.*, Antagonizing the alpha4beta1 integrin, but not alpha4beta7, inhibits leukocytic infiltration of the central nervous system in rhesus monkey experimental autoimmune encephalomyelitis. *J Immunol* **190**, 1961-1973 (2013).
57. B. E. Theien *et al.*, Discordant effects of anti-VLA-4 treatment before and after onset of relapsing experimental autoimmune encephalomyelitis. *J Clin Invest* **107**, 995-1006 (2001).
58. G. P. Rice, H. P. Hartung, P. A. Calabresi, Anti-alpha4 integrin therapy for multiple sclerosis: mechanisms and rationale. *Neurology* **64**, 1336-1342 (2005).
59. T. A. Yednock *et al.*, Prevention of experimental autoimmune encephalomyelitis by antibodies against alpha 4 beta 1 integrin. *Nature* **356**, 63-66 (1992).
60. J. L. Baron, J. A. Madri, N. H. Ruddle, G. Hashim, C. A. Janeway, Jr., Surface expression of alpha 4 integrin by CD4 T cells is required for their entry into brain parenchyma. *J Exp Med* **177**, 57-68 (1993).
61. N. A. Spidale *et al.*, Interleukin-17-Producing gammadelta T Cells Originate from SOX13(+) Progenitors that Are Independent of gammadeltaTCR Signaling. *Immunity* **49**, 857-872 e855 (2018).
62. Y. Ohoka, A. Yokota, H. Takeuchi, N. Maeda, M. Iwata, Retinoic acid-induced CCR9 expression requires transient TCR stimulation and cooperativity between NFATc2 and the retinoic acid receptor/retinoid X receptor complex. *J Immunol* **186**, 733-744 (2011).

674 63. A. Larange *et al.*, A regulatory circuit controlled by extranuclear and nuclear retinoic
675 acid receptor alpha determines T cell activation and function. *Immunity* **56**, 2054-2069
676 e2010 (2023).
677 64. N. Noy, Between death and survival: retinoic acid in regulation of apoptosis. *Annu Rev*
678 *Nutr* **30**, 201-217 (2010).
679 65. F. Da Silva *et al.*, Retinoic acid signaling is directly activated in cardiomyocytes and
680 protects mouse hearts from apoptosis after myocardial infarction. *eLife* **10**, (2021).
681 66. M. Iwata, M. Mukai, Y. Nakai, R. Iseki, Retinoic acids inhibit activation-induced
682 apoptosis in T cell hybridomas and thymocytes. *J Immunol* **149**, 3302-3308 (1992).
683 67. Y. Yang, M. S. Vacchio, J. D. Ashwell, 9-cis-retinoic acid inhibits activation-driven T-cell
684 apoptosis: implications for retinoid X receptor involvement in thymocyte development.
685 *Proc Natl Acad Sci U S A* **90**, 6170-6174 (1993).
686 68. F. Petermann *et al.*, gammadelta T cells enhance autoimmunity by restraining
687 regulatory T cell responses via an interleukin-23-dependent mechanism. *Immunity* **33**,
688 351-363 (2010).
689 69. C. A. Dendrou, L. Fugger, M. A. Friese, Immunopathology of multiple sclerosis. *Nat Rev*
690 *Immunol* **15**, 545-558 (2015).
691 70. M. Hiltensperger, T. Korn, The Interleukin (IL)-23/T helper (Th)17 Axis in
692 Experimental Autoimmune Encephalomyelitis and Multiple Sclerosis. *Cold Spring Harb*
693 *Perspect Med* **8**, (2018).
694 71. L. Schirmer, V. Rothhammer, B. Hemmer, T. Korn, Enriched CD161high CCR6+
695 gammadelta T cells in the cerebrospinal fluid of patients with multiple sclerosis. *JAMA*
696 *Neurol* **70**, 345-351 (2013).
697 72. J. van Langelaar *et al.*, T helper 17.1 cells associate with multiple sclerosis disease
698 activity: perspectives for early intervention. *Brain* **141**, 1334-1349 (2018).
699 73. E. Havrdova *et al.*, Activity of secukinumab, an anti-IL-17A antibody, on brain lesions in
700 RRMS: results from a randomized, proof-of-concept study. *J Neurol* **263**, 1287-1295
701 (2016).
702 74. C. Luckel *et al.*, IL-17(+) CD8(+) T cell suppression by dimethyl fumarate associates
703 with clinical response in multiple sclerosis. *Nature communications* **10**, 5722 (2019).
704 75. V. Cipollini, J. Anrather, F. Orzi, C. Iadecola, Th17 and Cognitive Impairment: Possible
705 Mechanisms of Action. *Front Neuroanat* **13**, 95 (2019).
706 76. V. Brucklacher-Waldert *et al.*, Tbet or Continued RORgammat Expression Is Not
707 Required for Th17-Associated Immunopathology. *J Immunol* **196**, 4893-4904 (2016).
708 77. K. Hirota *et al.*, Fate mapping of IL-17-producing T cells in inflammatory responses. *Nat*
709 *Immunol* **12**, 255-263 (2011).
710 78. C. Klemann *et al.*, Synthetic retinoid AM80 inhibits Th17 cells and ameliorates
711 experimental autoimmune encephalomyelitis. *Am J Pathol* **174**, 2234-2245 (2009).
712

Main Figures

Figure 1. RA sustains multiple transcriptional programs during γδT17 cell development

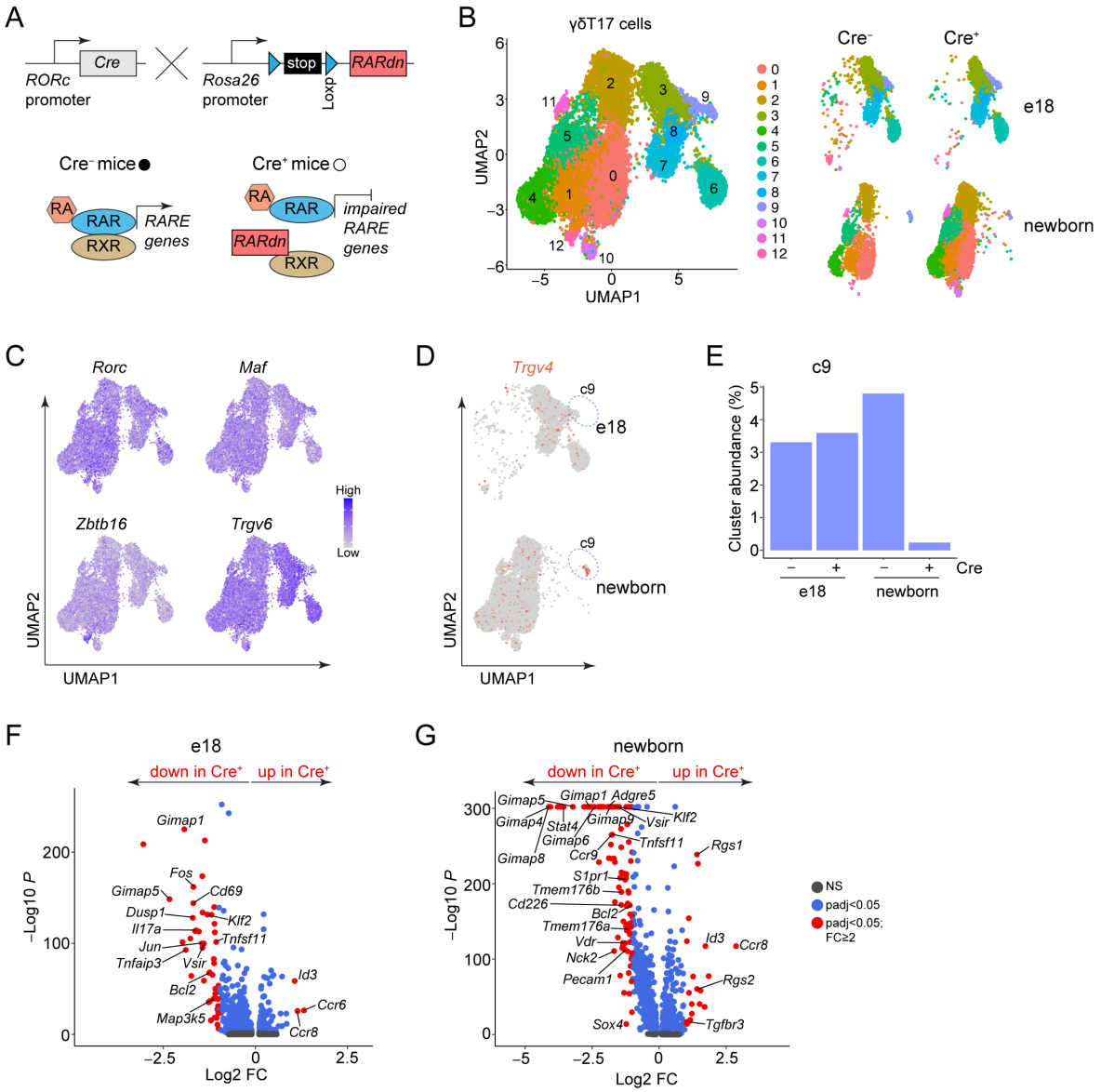

Figure 1. RA sustains multiple transcriptional programs during γδT17 cell development. (**A**) Schematic representation of the mouse model. RORγt^{CRE}-mediated expression of the RARdn transgene prevents RARα from interacting with RXR and thus cannot initiate its transcriptional activity. (**B**) UMAP plot displaying integrated e18 and newborn γδT17 thymocytes from transgenic (Cre^{+}) and littermate control (Cre^{-}) mice after unsupervised clustering (left) and UMAP split based on genotype and timepoint (right). (**C**) Feature plots illustrating the distribution and expression levels of *Rorc*, *Maf*, *Zbtb16* and *Trgv6*. (**D**) Feature plot for *Trgv4* expression split based on timepoint with cluster c9 circled. (**E**) Proportions of cluster c9 within each timepoint and genotype, shown as a fraction of the total γδT17 cell population. (**F-G**) Volcano plots for DEGs determined using a Wilcoxon Rank Sum test between Cre^{+} and Cre^{-} cells for e18 (**F**) and newborn cells (**G**). NS: not significant; FC: fold change; $\log_2$FC = 1, representing a fold change of at least 2. Selected DEGs are labeled on the plot.

Figure 2. RA strengthens the TCR signal during embryonic γδT17 cell development

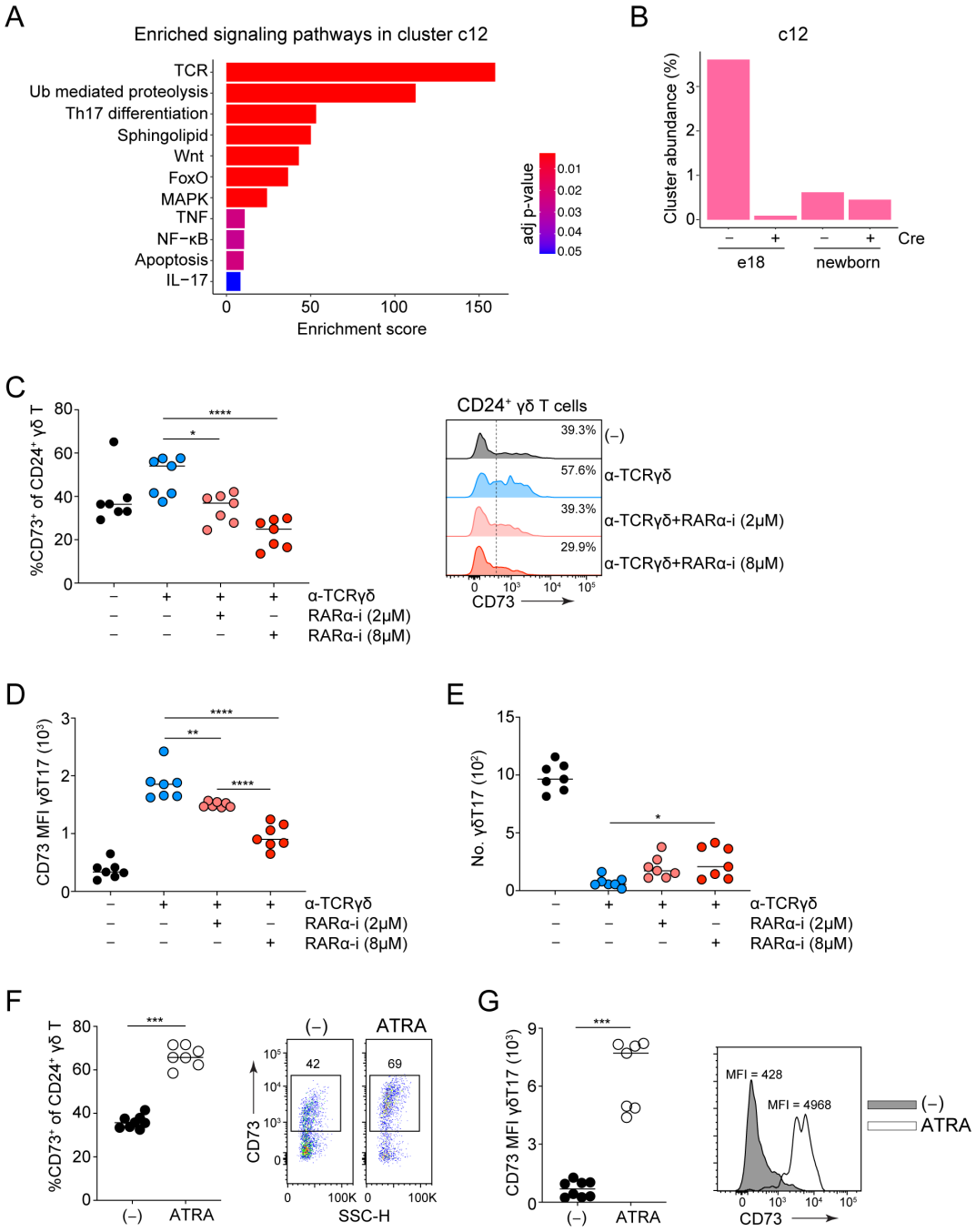

Figure 2. RA strengthens the TCR signal during embryonic γδT17 cell development. (**A**) KEGG pathway enrichment analysis of DEGs in cluster c12 compared to all other clusters performed using enrichR. Pathways are color-coded by adjusted p-value, with red indicating greater statistical significance. The combined enrichment score is shown on the x-axis. (**B**) Proportions of cluster c12 within each timepoint and genotype shown as a fraction of the total γδT17 cell population. (**C-E**) FTOCs were set up as described in **Fig. S1F** and were treated with α-TCRδ in the presence or absence of 2 and 8 μM RARα inhibitor (RARα-i). Frequencies of CD73^{+} cells within the immature (CD24^{+}) γδ T cell population across the different treatment combinations (left), and representative ridgeline plots of CD73 staining (right) (**C**). MFI of CD73 staining in the γδT17 cell population (**D**). Numbers of γδT17 cells in the FTOCs across the treatments (**E**). (**F-G**)

741 In separate experiments, FTOCs were treated with 160 nM of ATRA or left as untreated controls
742 (−). Frequency of $CD73^+$ cells in the $CD24^+$ γδ T population (left) and representative FACS plots of
743 CD73 staining of the same population (right) (**F**). MFI quantification of CD73 staining in γδT17 cells
744 (left) and representative histogram of CD73 staining of the same population (right) (**G**). In (**C-G**)
745 each symbol represents 2-3 thymic lobes pooled and the line the median; data are pool of two
746 experiments; p-values were determined using One-Way ANOVA with Tukey's multiple
747 comparisons test for **C-E** and Mann–Whitney test for **F-G**; *P < 0.05. **P < 0.01; ***P < 0.001;
748 ****P < 0.0001.
749

Figure 3. RA promotes survival and represses apoptosis of neonatal γδT17 cells

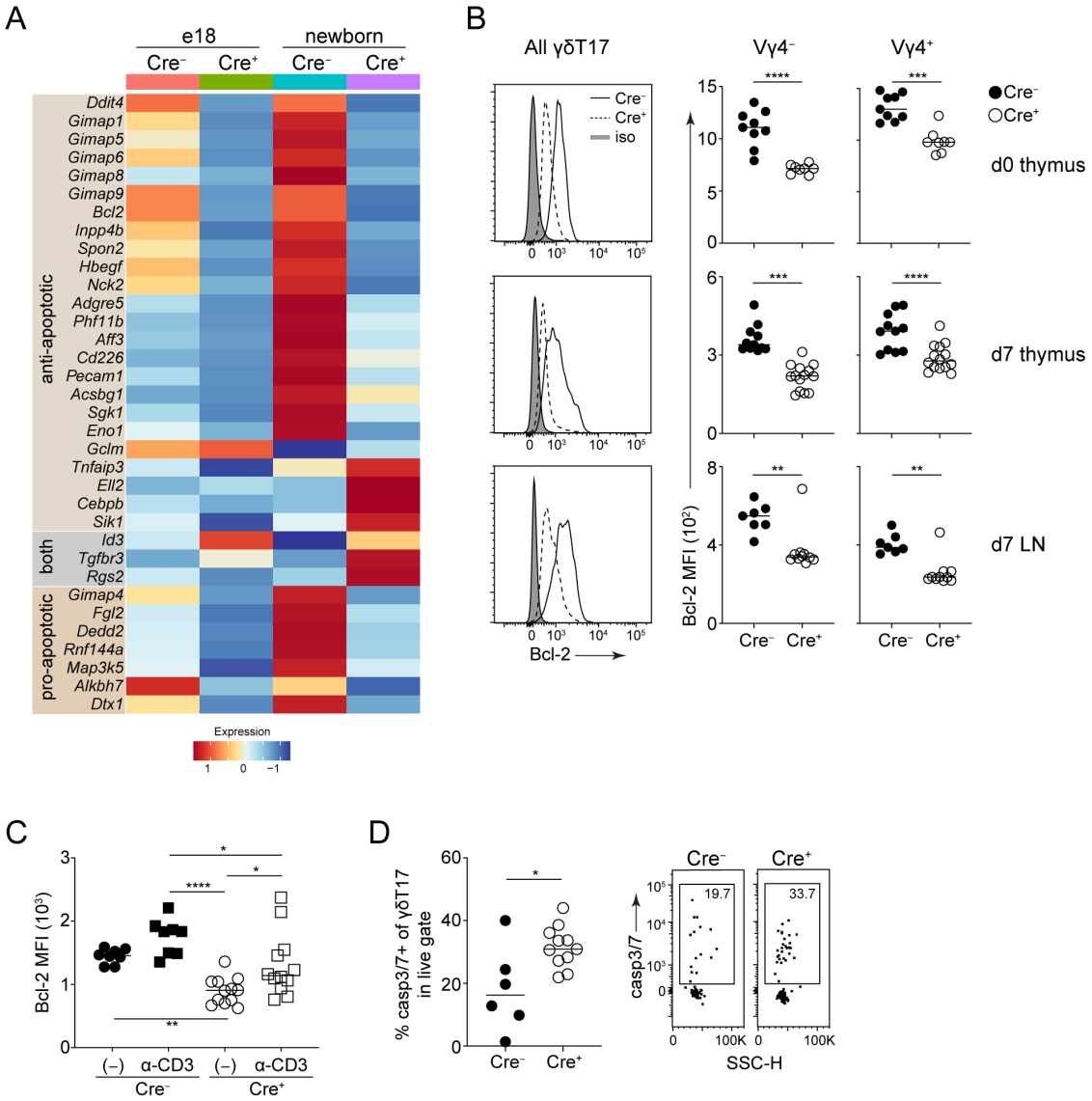

Figure 3. RA promotes survival and represses apoptosis of neonatal γδT17 cells. (**A**) Heatmap representation of selected DEGs between Cre⁻ and Cre⁺ cells for each timepoint grouped as anti-apoptotic, pro-apoptotic or both (**Table S3**). Colors indicate scaled gene expression levels, with red representing higher expression. (**B**) Quantification of Bcl-2 by flow cytometry for newborn (d0) thymus and neonatal (d7) thymus and lymph node (LN). Data is shown as representative histograms for γδT17 cells (left) and quantified individually for Vγ4⁻ and Vγ4⁺ cells within the γδT17 population. (**C**) MFI of Bcl-2 after overnight culture of newborn Cre⁻ and Cre⁺ thymocytes in the absence (−) or presence of 1 μg/ml α-CD3. (**D**) Frequency of caspase 3/7⁺ cells among the live γδT17 population following 40 hours of culture, along with a representative FACS plot (right). In (**B-D**) each symbol represents one mouse and the line the median; data are pool of three experiments; p-values were determined using One-Way ANOVA with Tukey's multiple comparisons test for **C** and Mann–Whitney test for **B** and **D**. *P < 0.05; **P < 0.01; ***P < 0.001; ****P < 0.0001.

Figure 4. RA induces activation, survival and interferon gene signatures in inflammation

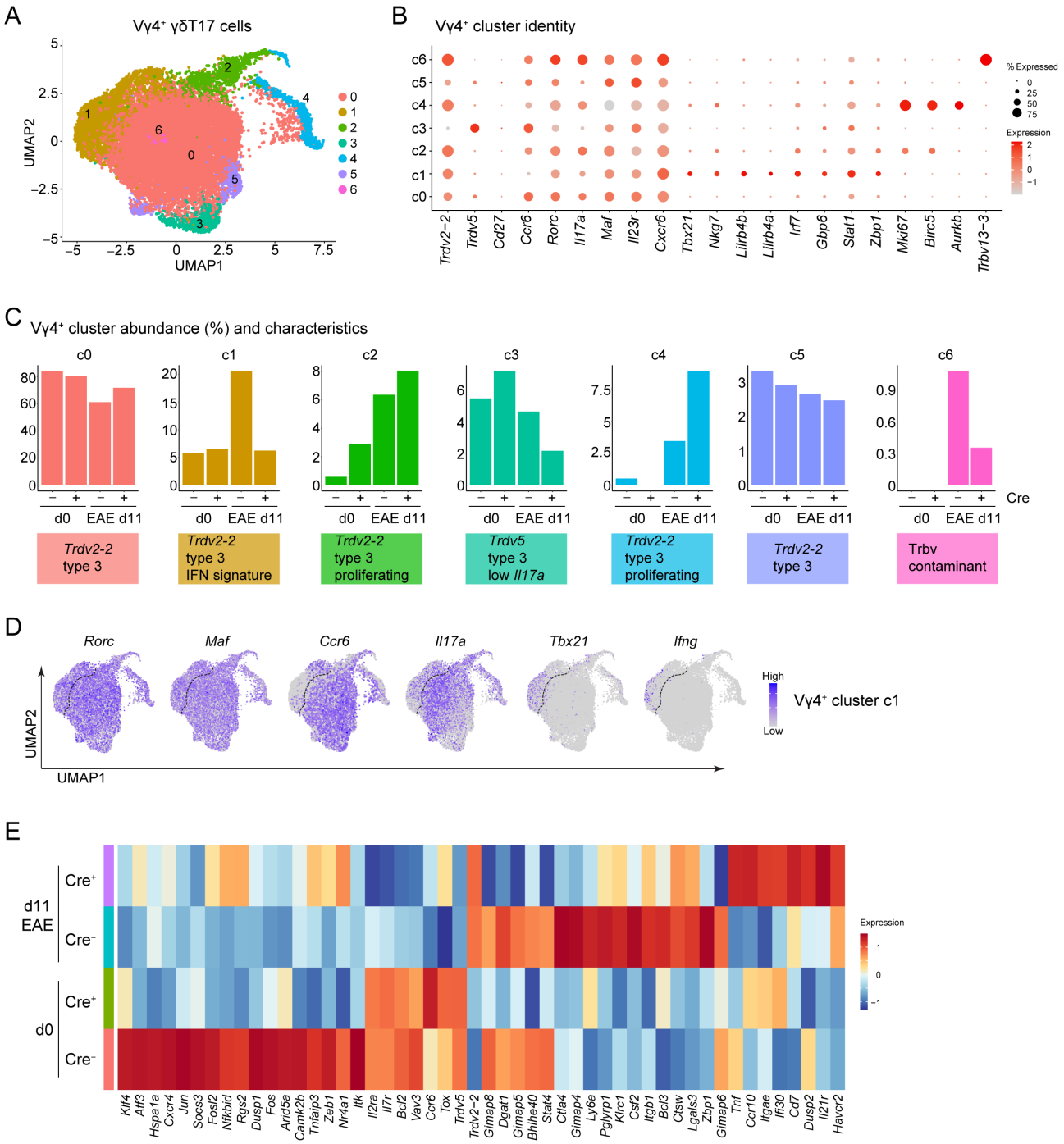

Figure 4. RA induces activation, survival and interferon gene signatures in inflammation. (**A**) UMAP of Vγ4⁺ γδT17 clusters integrated from the spleen of Cre⁻ and Cre⁺ mice before (d0) and 11 days (d11) after MOG_{35-55} immunization. (**B**) Dot plot showing the scaled expression of selected genes across clusters, with red representing higher expression. Dot size indicates the percentage of cells within each cluster expressing the corresponding gene. (**C**) Cluster characterization and abundance within each genotype and timepoint, shown as a fraction of all Vγ4⁺ cells. (**D**) Feature plots illustrating the distribution and expression levels of *Rorc*, *Maf*, *Ccr6*, *Il17a*, *Tbx21* and *Ifng*. A line is drawn to delineate the IFN signature cluster c1 from the others. (**E**)

776 Heatmap representation of selected DEGs between Cre^- and Cre^+ cells for each EAE timepoint.
777 Colors indicate scaled gene expression levels, with red representing higher expression.
778

Figure 5. RA is necessary for EAE mediated neuroinflammation

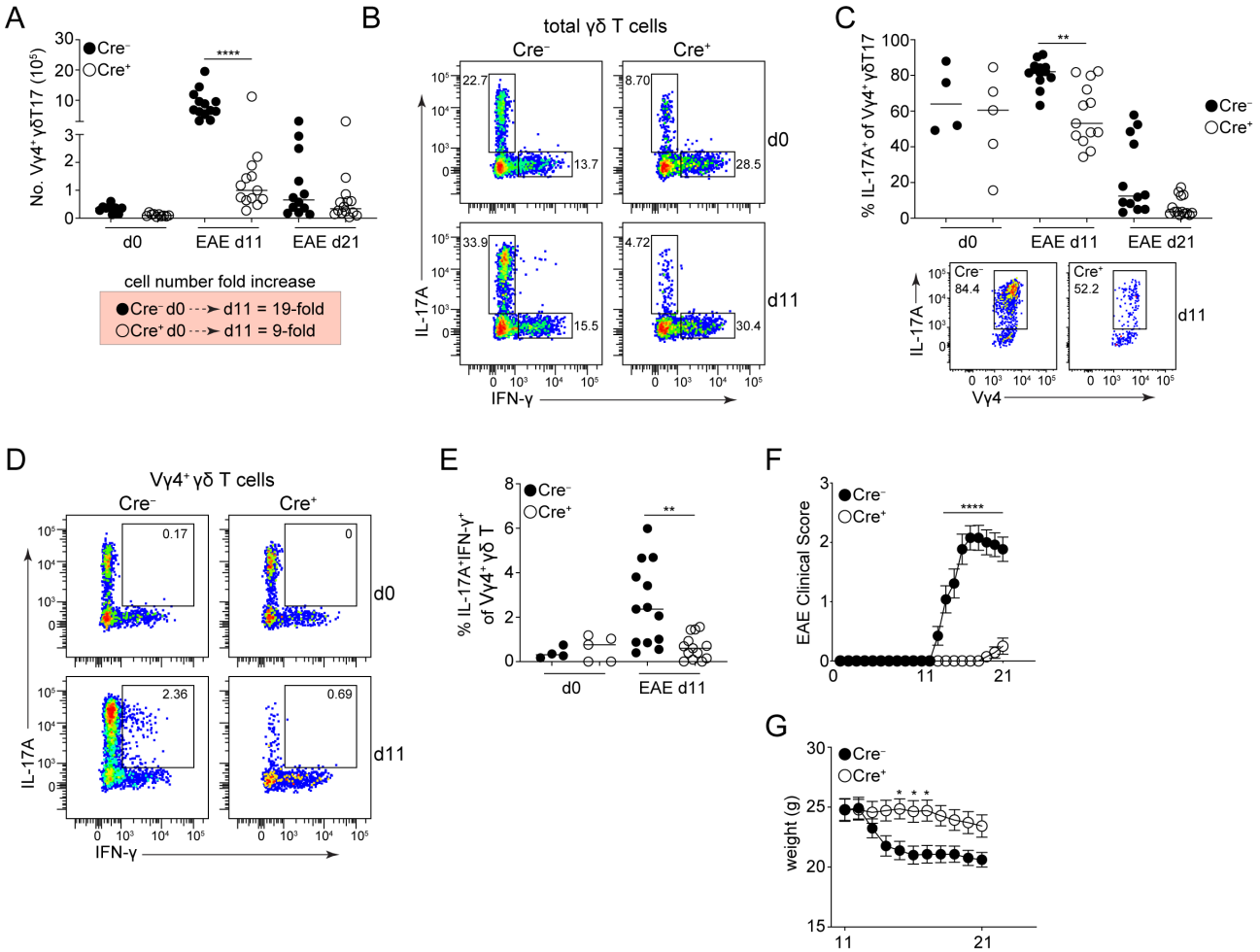

Figure 5. RA is necessary for EAE mediated neuroinflammation.

(**A**) Numbers of Vγ4$^+$ γδT17 cells in the spleen at d0, d11 and d21 after MOG_{35-55} immunization. The fold increase in cell numbers from d0 to d11 for each genotype is also shown. (**B**) Representative FACS plot showing IL-17A and IFN-γ cytokine production in the spleen within the total γδ T cell population at d0 and d11. (**C**) Frequency of IL-17A$^+$Vγ4$^+$ cells within the γδT17 population at different timepoints of EAE. Representative FACS plot for the IL-17A staining is also shown. (**D**) Representative FACS plots for IL-17A and IFN-γ co-production in the spleen by Vγ4$^+$ γδ T cells. (**E**) Frequency of IL-17A$^+$IFN-γ$^+$ cells within the Vγ4$^+$ γδ T cell population. (**F**) Disease progression measured by clinical symptoms until day 21 post immunization. (**G**) Mouse weight between d11 and d21. In **F** and **G** data are a pool of 13 (Cre$^-$) or 14 (Cre$^+$) mice and shown as mean±sem. Statistical analysis was performed using 2-way ANOVA with Bonferroni's multiple comparisons test. For all the other plots, each symbol represents a mouse and the line the median; data are a pool of three experiments; p-values were determined using One Way ANOVA with Tukey's multiple comparisons test. *P < 0.05; **P < 0.01; ****P < 0.0001.

Figure 6. RA is required for α4β1 expression and cell infiltration to the brain

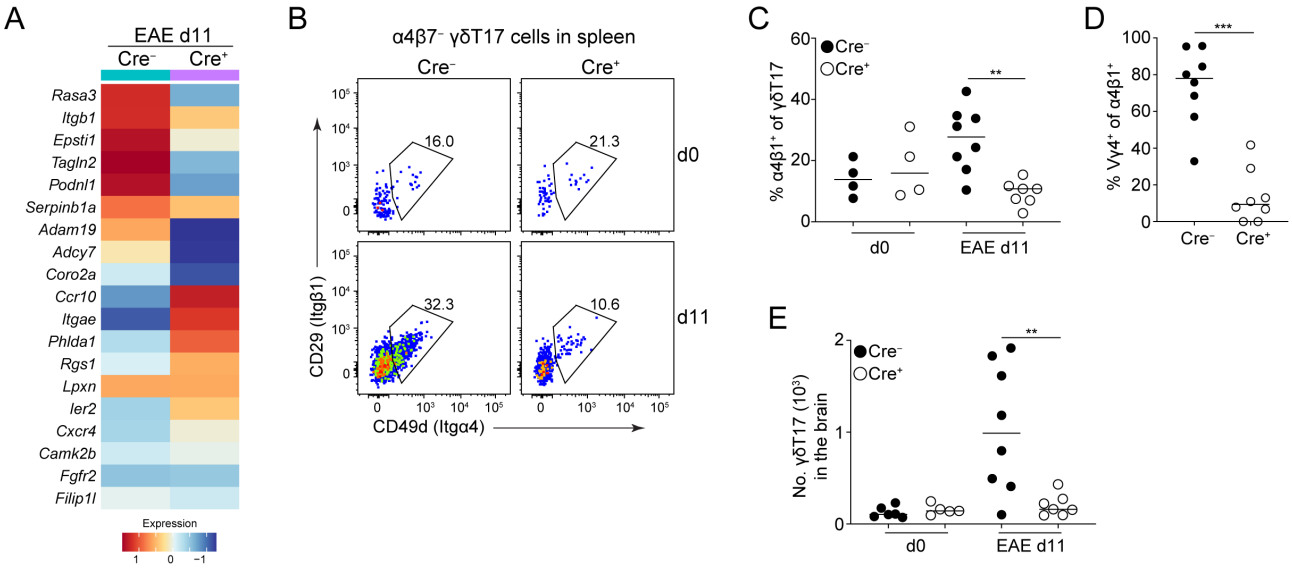

Figure 6. RA is required for α4β1 expression and γδT17 cell infiltration to the brain. (**A**) Heatmap representation of selected DEGs with potential roles in migration (**Table S6**) between Cre⁻ and Cre⁺ Vγ4⁺ cells at d11. Colors indicate scaled gene expression levels, with red representing higher expression. (**B**) Representative FACS plots of α4β1 integrin expression on splenic γδT17 cells at d0 and d11 of EAE (cells were pre-gated as α4β7⁻). (**C**) Frequency of α4β1⁺ cells within the γδT17 population. (**D**) Frequency of Vγ4⁺ cells within the α4β1⁺ γδT17 population at d11 of EAE. (**E**) Numbers of γδT17 cells in the brain of Cre⁻ and Cre⁺ at d0 and d11 of EAE. In all graphs, each symbol represents one mouse; data are pool of two experiments; p-values were determined using One-Way ANOVA with Tukey's multiple comparisons test for **C** and **E**, and Mann–Whitney test for **D**. *P < 0.05; **P < 0.01; ***P < 0.001.

Supplementary Figures

Figure S1. RA limits the development of γδT17 cells

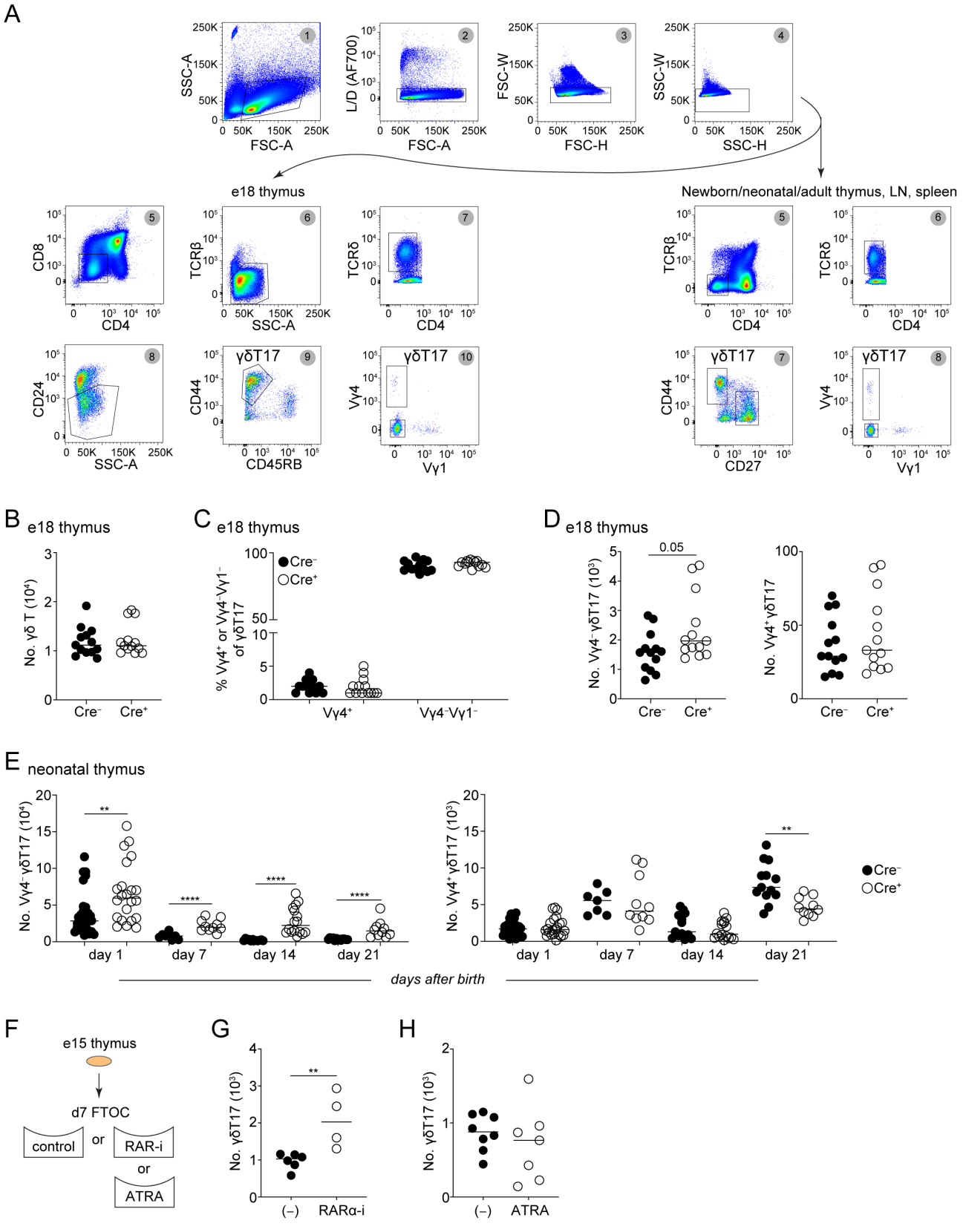

814 **Figure S1. RA limits the development of γδT17 cells.**

815 (**A**) Sequential gating for the identification and enumeration of γδT17 cell populations in the
816 embryonic thymus (left) and in all other neonatal and adult organs (right). (**B**) Numbers of total Cre^{-}
817 and Cre^{+} γδ T cells at e18. (**C**) Frequency of $V\gamma4^{+}$ and $V\gamma4^{-}V\gamma1^{-}$ cells within the γδT17 population
818 at e18. (**D**) Numbers of $V\gamma4^{-}$ (left) and $V\gamma4^{+}$ (right) cells within the γδT17 population at e18. (**E**)
819 Numbers of $V\gamma4^{-}$ (left) and $V\gamma4^{+}$ (right) cells within the γδT17 population in the thymus at the
820 indicated days after birth. (**F**) Schematic representation of the fetal thymic organ cultures (FTOCs).
821 (**G-H**) Numbers of γδT17 cells in FTOCs that were treated with 8 μM RARα inhibitor (RARα-i) (**G**)
822 or 160 nM of ATRA (**H**). In all graphs, each symbol represents one mouse (**B-E**) or 2-3 thymic
823 lobes pooled (**G-H**); data are pool of three (**B-E**) or two (**G-H**) experiments; p-values were
824 determined using Mann–Whitney test. **$P < 0.01$; ***$P < 0.001$.

825

Figure S2. RA regulates the numbers of γδT17 cells in neonatal and adult life

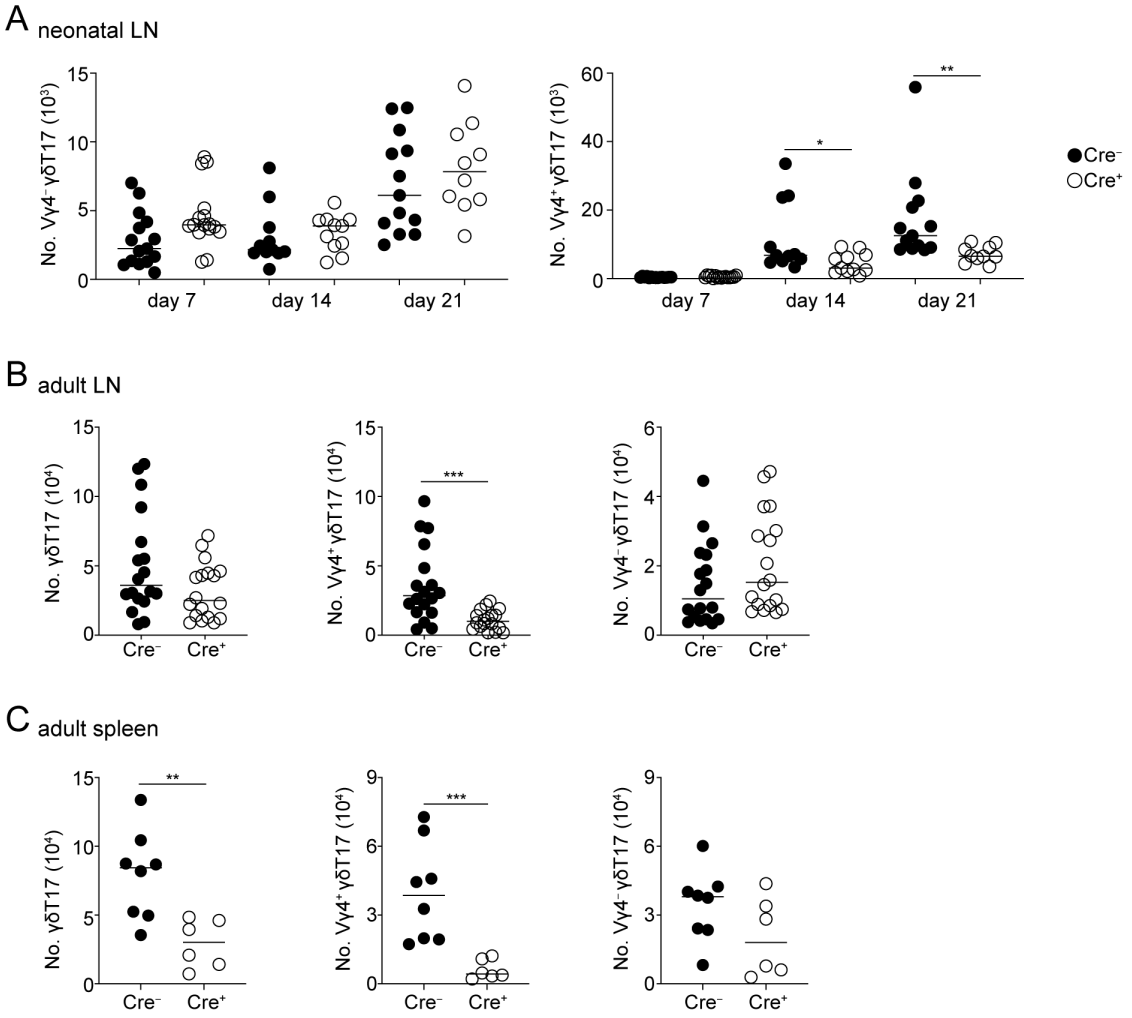

Figure S2. RA regulates the numbers of γδT17 cells in neonatal and adult life. (**A**) Numbers of Vγ4⁻ (left) and Vγ4⁺ (right) γδT17 cells in the LNs at the indicated days after birth. (**B-C**) Numbers of total γδT17 (left), Vγ4⁺ γδT17 (middle) and Vγ4⁻ γδT17 (right) cells in the LN and spleen (**C**) of adult Cre⁻ and Cre+ mice. In all graphs, each symbol represents one mouse; data are pool of three experiments; p-values were determined using Mann–Whitney test. *P < 0.05; **P < 0.01; ***P < 0.001.

Figure S3. RA induces activation, survival and interferon gene signatures during inflammation

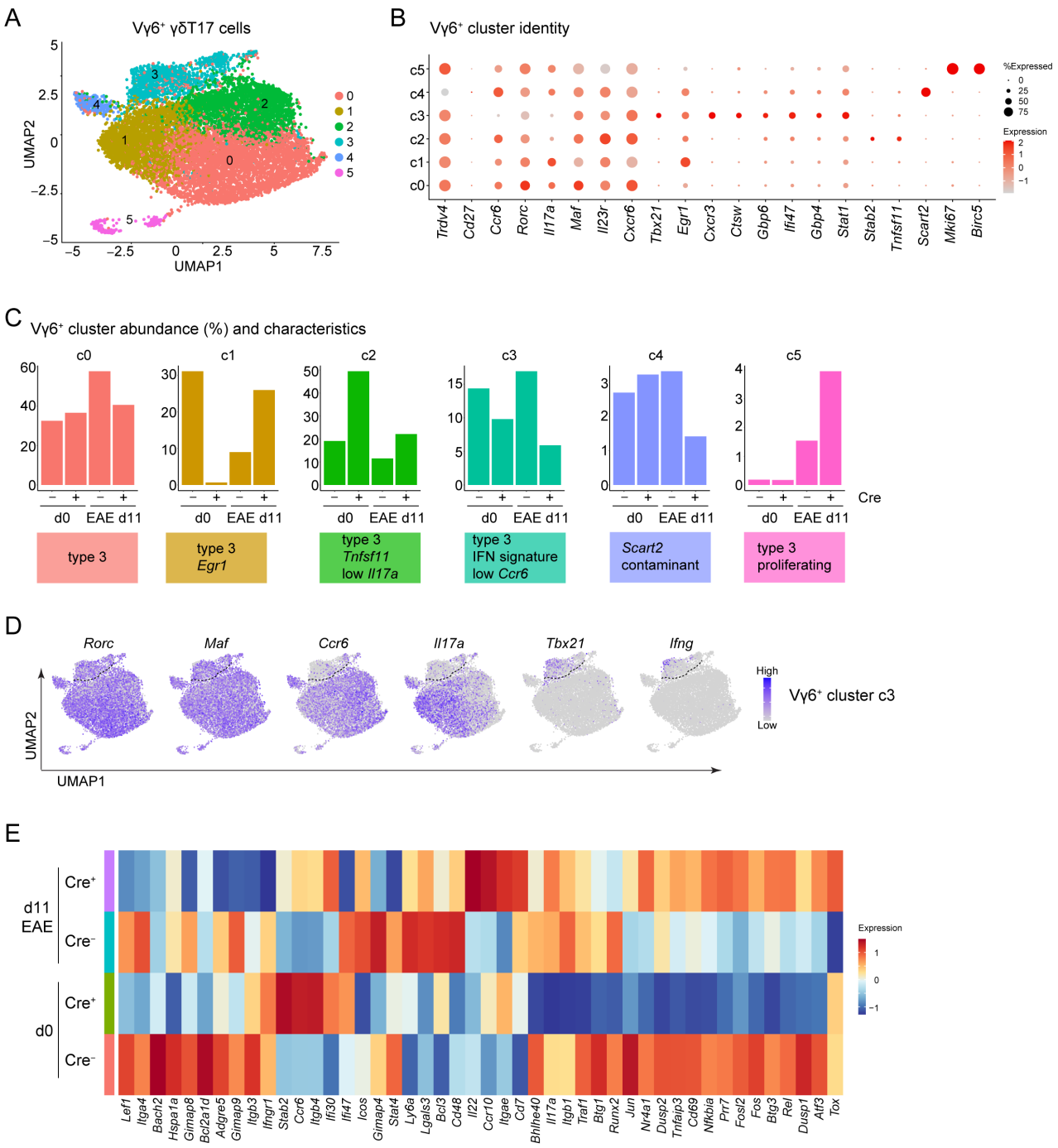

Figure S3. RA induces activation, survival and interferon gene signatures in inflammation. (**A**) UMAP of Vγ6⁺ γδT17 clusters, integrated from the spleen of Cre⁻ and Cre⁺ mice before (d0) and 11 days (d11) after MOG_{35-55} immunization. (**B**) Dot plot showing the scaled expression of selected genes across clusters, with red representing higher expression. Dot size indicates the percentage of cells within each cluster expressing the corresponding gene. (**C**) Cluster characterization and abundance within each genotype and timepoint, shown as a fraction of all Vγ6⁺ cells. (**D**) Feature plots illustrating the distribution and expression levels of *Rorc*, *Maf*, *Ccr6*, *Il17a*, *Tbx21* and *Ifng*. A line is drawn to delineate the IFN signature cluster c3 from the others. (**E**)

845 Heatmap representation of selected DEGs between Cre^- and Cre^+ cells for each EAE timepoint.
846 Colors indicate scaled gene expression levels, with red representing higher expression.

Figure S4. γδ and CD4 T cell responses during EAE

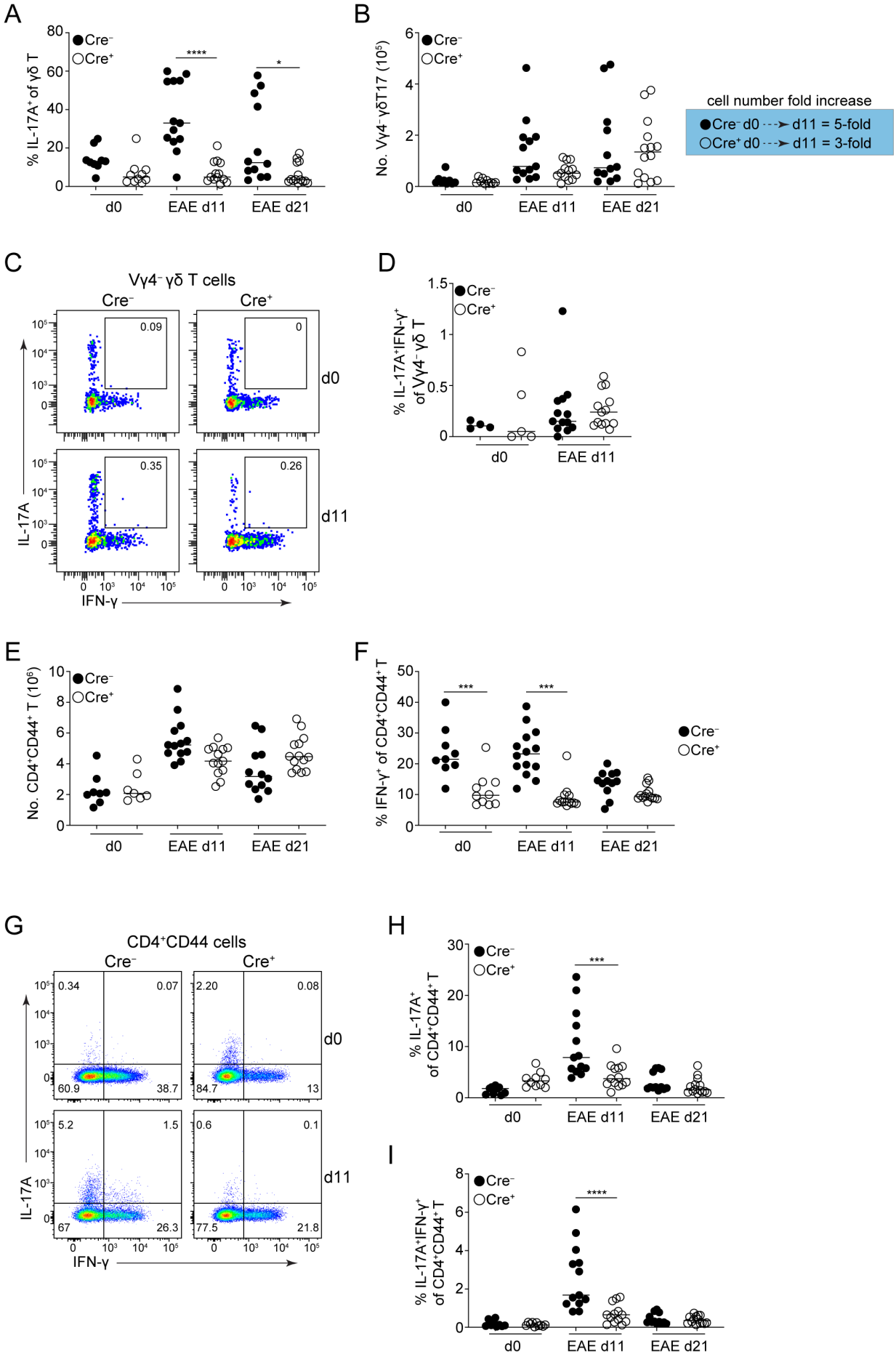

847

848 **Figure S4. γδ and CD4 T cell responses during EAE.**

849 (**A**) Frequency of IL-17A$^+$ γδ T cells in the spleen at d0, d11 and d21 of EAE. (**B**) Number of Vγ4$^-$
850 cells within the γδT17 population in the spleen at different timepoints of EAE. On the right, the fold
851 increase in cell numbers from d0 to d11 is displayed for each genotype. (**C**) Representative FACS
852 plots for IL-17A and IFN-γ co-production in the spleen by Vγ4$^-$ γδ T cells. (**D**) Frequency of IL-
853 17A$^+$IFN-γ$^+$ cells within the Vγ4$^-$ γδ T cell population. (**E**) Number of splenic CD4$^+$CD44$^+$ T cells at
854 d0, d11 and d21 of EAE. (**F**) Frequency of IFN-γ$^+$ cells within the CD4$^+$CD44$^+$ T cell population at
855 different timepoints of EAE. (**G**) Representative FACS plots for IL-17A and IFN-γ production in the
856 spleen by activated (CD44$^+$) Cre$^-$ and Cre$^+$ CD4$^+$ T cells at d0 and d11. (**H-I**) Frequency of IL-17A$^+$
857 (**H**) and IL-17A$^+$IFN-γ$^+$ (**I**) cells within the CD4$^+$CD44$^+$ T cell population at different EAE timepoints.
858 For all plots, each symbol represents a mouse and the line the median; data are pool of three
859 experiments; p-values determined using One Way ANOVA with Tukey's multiple comparisons test.
860 *P < 0.05; ***P < 0.001; ****P < 0.0001.
861

Figure S5. RA is required for α4β1 expression and cell infiltration to the brain

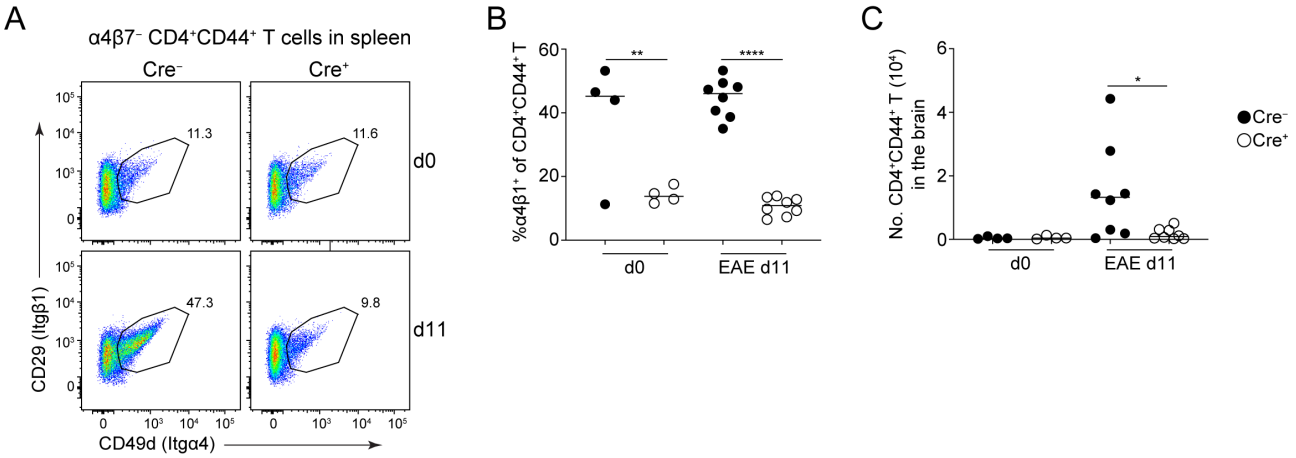

Figure S5. RA is required for α4β1 expression and cell infiltration to the brain. (**A**) Representative FACS plots of α4β1 integrin expression on splenic $CD4^+CD44^+$ T cells at d0 and d11 of EAE (cells were pre-gated as $\alpha4\beta7^-$). (**B**) Frequency of $\alpha4\beta1^+$ cells within the $CD4^+CD44^+$ T cell population. (**C**) Numbers of $CD4^+CD44^+$ T cells in the brain of Cre^- and Cre^+ at d0 and d11 of EAE. In all graphs, each symbol represents one mouse; data are pool of two experiments; p-values determined using One Way ANOVA with Tukey's multiple comparisons test. *P < 0.05; **P < 0.01; ****P < 0.0001.